Geochemistry Geophysics Geosystems G3
AN ELECTRONIC JOURNAL OF THE EARTH SCIENCES
Published by AGU and the Geochemical Society

Article
Volume 7, Number 5
11 May 2006
Q05015, doi:10.1029/2005GC001123
ISSN: 1525-2027

Asymmetric plume-ridge interaction around Iceland: The Kolbeinsey Ridge Iceland Seismic Experiment

Emilie E. E. Hooft
Department of Geological Sciences, University of Oregon, 1272 Cascade Hall, Eugene, Oregon 97403, USA (emilie@uoregon.edu)

Bryndís Brandsdóttir
Institute of Earth Sciences, University of Iceland, Öskju, Sturlugöta 7, IS-101 Reykjavík, Iceland

Rolf Mjelde
Department of Earth Science, University of Bergen, Allegaten 41, N-5007 Bergen, Norway

Hideki Shimamura
Musashino-gakuin University, 860 Kamihirose Sayama-shi, Saitama, 350-1321 Japan

Yoshio Murai
Institute for Seismology and Volcanology, Hokkaido University, N10S8 Kita-ku, Sapporo, 060-0810 Japan

[1] We present the results of a seismic refraction experiment that constrains crustal structure and thickness along 225 km of the Kolbeinsey Ridge and Tjörnes Fracture Zone and thus quantifies the influence of the Iceland hot spot on melt flux at the spreading center north of Iceland. North of the Iceland shelf, crustal thickness is relatively constant over 75 km, 9.4 ± 0.2 km. Along the southern portion of the Kolbeinsey Ridge, on the Iceland shelf, crustal thickness increases from 9.5 ± 0.1 km to 12.1 ± 0.4 km over 90 km. Gravity inversion indicates a residual crustal gravity anomaly that decreases by about 30–40 mGal toward Iceland. We infer that the variations in crustal thickness and gravity are accompanied by mantle temperature changes of 40° to 50°C. At similar distances from the Iceland hot spot, crustal thickness along the Kolbeinsey Ridge is 2–2.5 km less than at the Reykjanes Ridge, consistent with the asymmetry in plume-ridge interaction that has been inferred from the axial depth and geochemistry of these ridges. Average lower crustal velocities are also higher along the Kolbeinsey Ridge, consistent with a lower degree of active upwelling than along the Reykjanes Ridge. Topography and crustal thickness patterns at the spreading centers around Iceland are consistent with isostatic support for normal crustal and mantle densities. However, we infer that the lower crust beneath central Iceland is considerably denser than that beneath the adjacent ridges. Crustal thickness and geochemical patterns suggest that deep melting is spatially limited and asymmetric about Iceland while shallow melting is enhanced over a broad region. This asymmetry may be due to a mantle plume that is tilted from south to north in the upper mantle and preferentially melts deeper enriched material beneath the Reykjanes Ridge.

Components: 13,520 words, 15 figures, 4 tables.

Keywords: Iceland; oceanic crust; plume-ridge interaction.

Index Terms: 7245 Seismology: Mid-ocean ridges; 7220 Seismology: Oceanic crust; 8137 Tectonophysics: Hotspots, large igneous provinces, and flood basalt volcanism.

Received 22 August 2005; **Revised** 25 October 2005; **Accepted** 9 February 2006; **Published** 11 May 2006.

Hooft, E. E. E., B. Brandsdóttir, R. Mjelde, H. Shimamura, and Y. Murai (2006), Asymmetric plume-ridge interaction around Iceland: The Kolbeinsey Ridge Iceland Seismic Experiment, *Geochem. Geophys. Geosyst.*, *7*, Q05015, doi:10.1029/2005GC001123.

1. Introduction

[2] The influence of the Iceland hot spot on the adjacent ridges, has been recognized since the 1970s and extends more than 1,000 km away from the plume's center [*Cochran and Talwani*, 1978; *Haigh*, 1973; *Schilling*, 1973b; *Schilling et al.*, 1983; *Talwani and Eldholm*, 1977; *Vogt*, 1983] (Figure 1). Recent passive seismic investigations provide evidence for a plume-like structure that extends through the upper mantle and possibly into the lower mantle [*Allen et al.*, 1999; *Foulger et al.*, 2000; *Hung et al.*, 2004; *Shen et al.*, 1998; *Wolfe et al.*, 1997]. Major and trace element studies at Iceland and along the Reykjanes (RR) and Kolbeinsey Ridges (KR) to the south and north, respectively, support a decreasing extent of melting with distance from the plume [*Klein and Langmuir*, 1987; *Schilling*, 1999; *Shen and Forsyth*, 1995; *White et al.*, 1995]. In addition, along-axis gradients in trace elements and isotope compositions suggest mixing between plume and normal mid-ocean ridge basalt sources [*Blichert-Toft et al.*, 2005; *Graham*, 2002; *Hanan and Schilling*, 1997; *Hart et al.*, 1973; *Mertz et al.*, 1991; *Poreda et al.*, 1986; *Schilling*, 1973a, 1999]. Seismic measurements of crustal thickness along Iceland's neovolcanic zone and the adjacent mid-ocean ridges also support a decreasing extent of melt production with distance from the center of the plume [e.g., *Allen et al.*, 1999; *Bjarnason et al.*, 1993; *Brandsdóttir et al.*, 1997; *Bunch and Kennett*, 1980; *Darbyshire et al.*, 1998; *Kodaira et al.*, 1997; *Navin et al.*, 1998; *Smallwood and White*, 1998; *Staples et al.*, 1997; *Weir et al.*, 2001].

[3] To first order, geodynamic models of plume-ridge interactions reproduce these variations in geochemical and geophysical observations [e.g., *Ito et al.*, 1996, 1999]; however, plume-ridge interactions show greater complexity. In particular, the Iceland-Mid-Atlantic Ridge (MAR) hot spot-ridge system exhibits a noticeable asymmetry in topography and geochemistry of the Reykjanes Ridge (RR) to the south compared to the Kolbeinsey Ridge (KR) north of Iceland (Figure 2). The ridge axis is more elevated along the RR (200–500 m), especially from 200 to 1000 km from the hot spot. He, Hf, Nd and Sr isotopic ratios along the KR and RR all reveal asymmetric mixing with an enriched and long-isolated source [*Blichert-Toft et al.*, 2005; *Graham*, 2002; *Mertz et al.*, 1991; *Poreda et al.*, 1986; *Schilling*, 1999]; the mixing halo covers about 1° of latitude along the KR and 5° of latitude along the RR. Elevated $^{3}He/^{4}He$ values are also asymmetric but extend to greater distances, 500 km along the KR and 1500 km along the RR [*Poreda et al.*, 1986]. A notable complexity is that Pb isotopic ratio patterns are decoupled from these other elements and differ markedly along the KR and RR with both $^{206}Pb/^{204}Pb$ and $^{208}Pb/^{204}Pb$ elevated along the RR [*Blichert-Toft et al.*, 2005; *Mertz et al.*, 1991; *Schilling*, 1999]. These data indicate that these ridges are interacting with different components of the Iceland plume and suggest a geochemically zoned plume [*Blichert-Toft et al.*, 2005].

[4] Different processes have been suggested to explain the observed asymmetry in the spreading centers north and south of Iceland including damming of plume outflow by lithospheric offsets or other high viscosity boundaries [*Georgen and Lin*, 2003; *Yale and Phipps Morgan*, 1998]; a mantle plume that spreads at greater depths to the north than to the south [*Mertz et al.*, 1991; *Schilling*, 1999] possibly due to the retarding effect of north-to-south asthenospheric flow on plume outflow north of Iceland [*Mertz et al.*, 1991]; and a plume that is tilted south to north in the upper mantle due either to northward flow of the Icelandic asthenosphere or southward flow of the upper part of the lower mantle [*Shen et al.*, 2002]. The asymmetry observed in hot spot-ridge systems provides an observational tool for understanding the interaction between actively upwelling mantle plumes and passive mantle upwelling beneath mid-ocean ridges.

[5] The Kolbeinsey Ridge Iceland Seismic Experiment (KRISE) measured variations in crustal thickness, as an indication of melt flux, on transects north of Iceland. This region is poorly studied and is critical to further refining geodynamic mod-

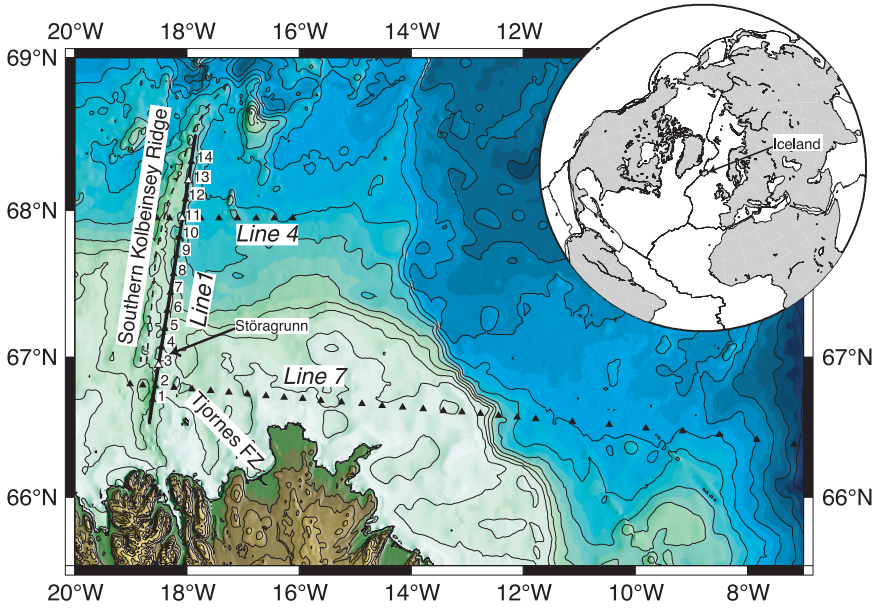

Figure 1. Location of KRISE seismic refraction experiment; see inset. Bathymetry at 200 m contour interval. Heavy black line is the north coast of Iceland. The axis of the southern Kolbeinsey Ridge (dashed line), the Tjörnes fracture zone, and the volcano Stóragrunn are marked. Refraction profiles 1, 4, and 7 are shown; OBSs, triangles (white for no data), are numbered for profile 1, and the shots are shown with a black line.

els of plume-ridge interaction at Iceland (Figure 3). North of Iceland there is only one crustal thickness measurement along the KR at 70°N [*Kodaira et al.*, 1997] and constraints on the past melt flux at the spreading center north of the plume, recorded in the thickness of off-axis oceanic crust are sparse [*Kodaira et al.*, 1997]. In this paper we present measurements of crustal structure and thickness along the Kolbeinsey Ridge north of Iceland. These data are used to invert gravity data for mantle density and temperature variations. We infer the mode of mantle upwelling north and south of Iceland from crustal thickness and average crustal velocity. Lastly, we investigate isostatic and dynamic support of topography.

2. Tectonic Setting of the Kolbeinsey Ridge

[6] Spreading along the Kolbeinsey Ridge was initiated at anomaly 6c time (~26 Ma) following a westward ridge jump from the extinct Ægir Ridge [*Appelgate*, 1997; *Jung and Vogt*, 1997; *Vogt et al.*, 1980]. The Kolbeinsey Ridge is bounded by the Tjörnes Fracture Zone to the south and the Jan Mayen Transform Fault to the north. Full spreading

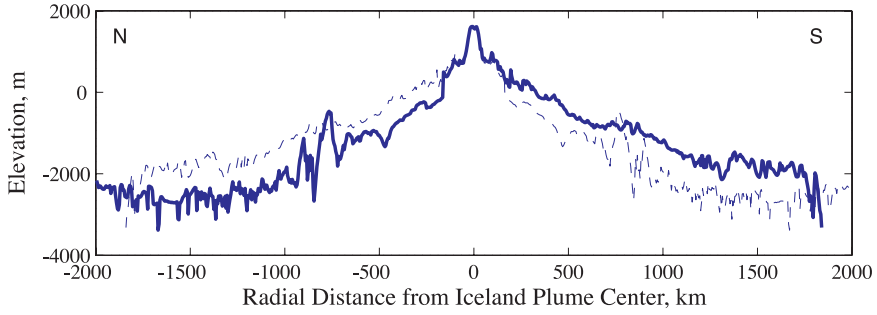

Figure 2. Elevation of the neovolcanic zone and spreading centers north and south of Iceland plotted as a function of radial distance from the Iceland plume center (heavy line). The dashed line shows the elevation mirrored about the plume center. Note the deeper bathymetry along the Kolbeinsey Ridge compared to the Reykjanes Ridge.

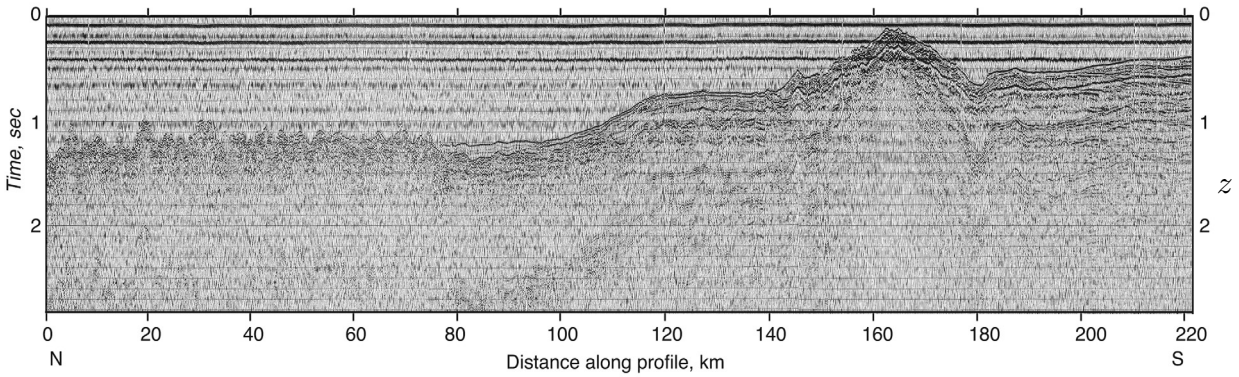

Figure 3. Reflection section from minihydrophone streamer. The data are band-pass filtered from 20 to 40 Hz with a 48 dB/oct drop-off and plotted with an AGC window of one second.

rates are slow and increased from 15 to 20 mm/yr at 12–13 Ma [*Appelgate*, 1997]. The Kolbeinsey Ridge axis was initially a continuous feature, however, short-lived rapidly migrating ridge offsets have existed since 7–8 Ma. The southern ridge axis, from the Tjörnes fracture zone at 66°50′N to the 34-km right-stepping Spar offset at 69°N, is clearly delineated by a continuous axial high (~30 km wide and ~500 m vertical relief) and a high-amplitude central magnetic anomaly [*Appelgate*, 1997; *Vogt et al.*, 1980]. Just south of the Spar offset, a smaller nontransform discontinuity offsets the ridge by 10 km in a right lateral sense at 68°43′N. Magnetic data show that this offset formed at ~5.5 Ma and has propagated northward through time. Thus the southern Kolbeinsey Ridge has lengthened to the north at a rate of ~100 mm/yr [*Appelgate*, 1997]. (This rate is similar to the southward propagation rate of the V-shaped anomalies on the Reykjanes Ridge.) At the southernmost part of the Kolbeinsey Ridge a fairly constant spreading rate during the last 10 Ma is inferred from the present location of magnetic anomaly 5 at the junction of the ridge with the Tjörnes Fracture Zone, similar to the current spreading rate of ~18 mm/yr, 105° [*DeMets et al.*, 1994].

[7] The junction of the Kolbeinsey Ridge axis with the Tjörnes Fracture Zone is located on the Iceland insular shelf. The Tjörnes Fracture Zone forms the offshore connection between the Kolbeinsey ridge and the rift zone in northern Iceland. It consists of two parallel seismically active lineaments, the Grímsey Rift Zone and the Húsavík-Flatey Fault, that are obliquely oriented (NW-SE). These two lineaments appear to accommodate both extension and shear. The Grímsey Rift Zone lies north of the Húsavík-Flatey Fault and is believed to have formed during the last 1–2 Ma in response to the northward propagation of the rift axis in northern Iceland [*Sæmundsson*, 1978]. It is made up of four left-stepping, en echelon, oblique rift segments akin to the volcanic systems on land. The largest segment is located adjacent to the Kolbeinsey ridge and consists of a large, shield-like volcano, Stóragrunn (~40 km^3) with a transecting rift zone (Figure 1).

[8] Several fjords and basins that were pathways of major outlet glaciers during recent glaciations incise the insular shelf of Iceland. The southernmost extension of the Kolbeinsey ridge is the Eyjafjarðaráll basin, which is by far the deepest basin on the Iceland shelf and extends down to 700 m depth. It is bounded by numerous NS-trending normal faults indicating that it is still actively extending with the ridge axis [*Brandsdóttir et al.*, 2001]. Seismic reflection data indicate a sedimentary thickness of up to 4 km within the Eyjafjarðaráll basin [*Gunnarsson*, 1998].

[9] There is only one seismic constraint on crustal thickness along the Kolbeinsey Ridge north of Iceland, which is located north of the Spar offset between 69°30′N and 70°20′N [*Kodaira et al.*, 1997]. These data show low velocities and significant lateral variations in the lower crust at the ridge axis. The crustal thickness at the axis varies from 7.2 to 11.4 km. Lower crustal velocities increase off axis and 12 km east of the ridge the crustal thickness is more uniform, 8 to 9 km. In contrast, there are several seismic constraints on crustal thickness along the Reykjanes Ridge [*Bunch and Kennett*, 1980; *Kodaira et al.*, 1997; *Navin et al.*, 1998; *Smallwood and White*, 1998;

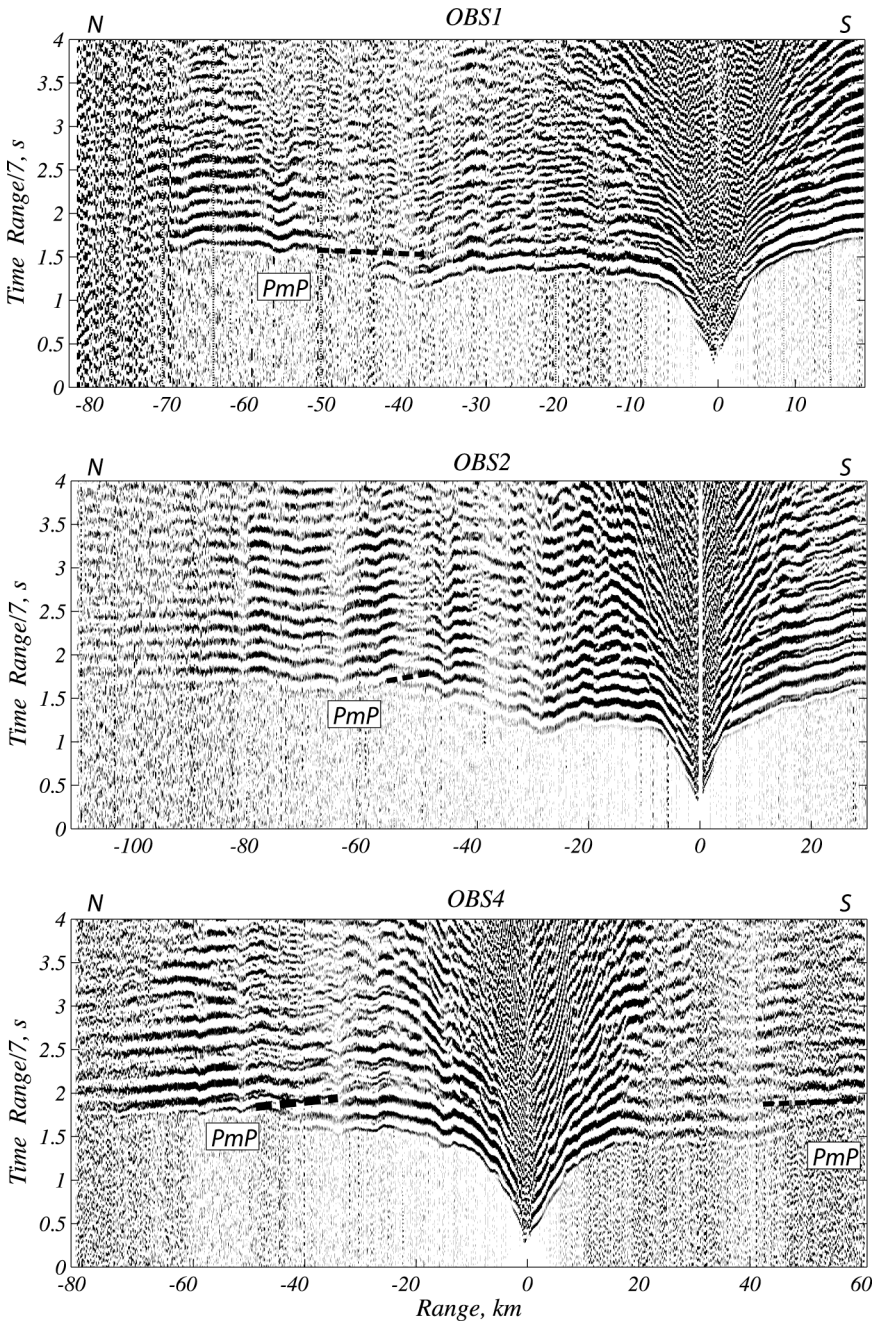

Figure 4a. Record sections of the refraction data from ocean bottom seismometers, OBS1, OBS2, and OBS4, plotted as reduced travel time (7 km/s) versus range. Data are band-pass filtered from 3 to 20 Hz and amplified as a function of range. Arrivals are observed out to over 100 km. Note the clear PmP arrivals on most stations.

Weir et al., 2001], which allow us to assess the asymmetry in melt flux between the KR and RR.

3. Seismic Experiment

[10] The KRISE experiment measured crustal refractions, P, and Moho reflections, PmP, along three profiles north of Iceland to constrain crustal structure and thickness (Figure 1). We also collected bathymetry, magnetic, gravity and ministreamer reflection data. We surveyed an along-axis profile, Profile 1, and two across-axis profiles, Profiles 4 and 7, located 180 and 70 km north of the Iceland coast, respectively. In this paper we analyze Profile 1, which is 225 km long and extends from just south of the 68°43′N nontransform discontinuity to the

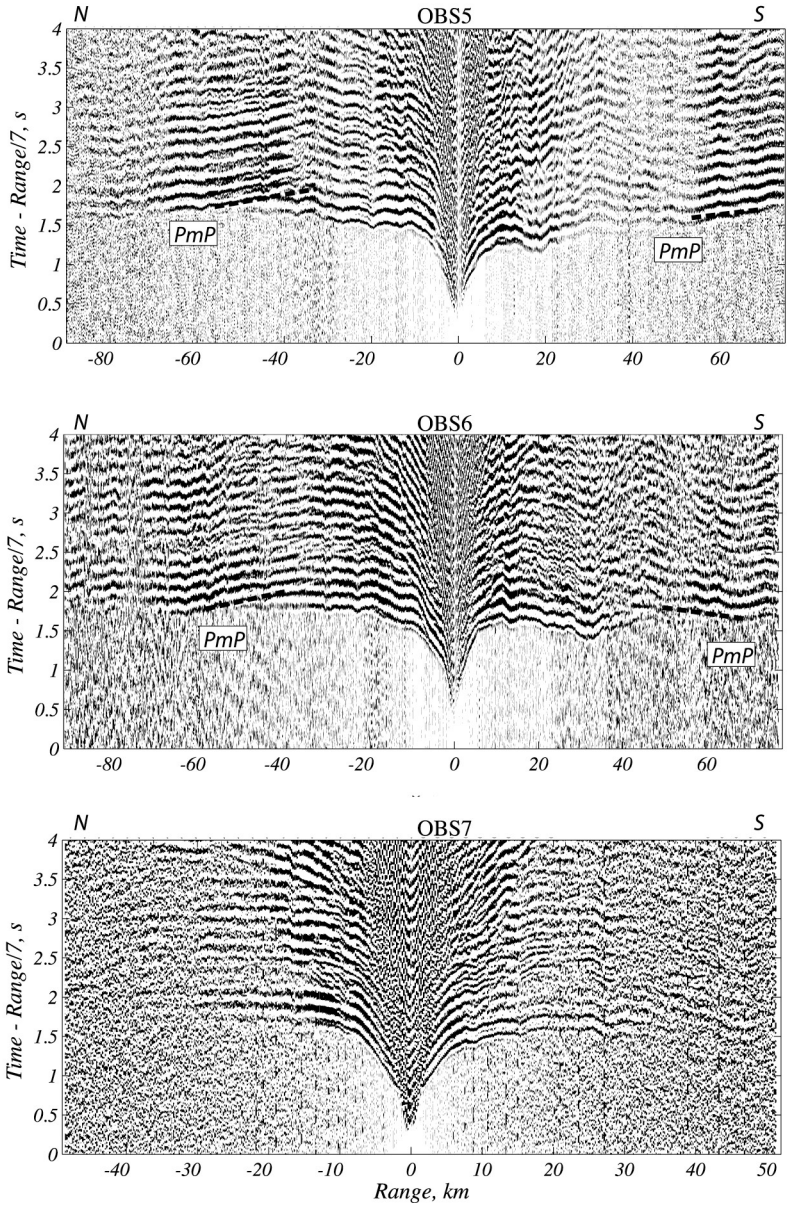

Figure 4b. Record sections for OBS5, OBS6, and OBS7, plotted as in Figure 4a.

KR-TFZ junction (68°30′N to 66°32′, Figure 1). This profile was shot about 7 km east of the axis of the Kolbeinsey Ridge to ensure good PmP arrivals by avoiding any low velocity zones (high attenuation) and rough topography at the ridge axis. Profile 1 starts in the deep water north of the Iceland insular shelf, crosses the edge of the Iceland platform and passes directly over the most pronounced volcanic system (Stóragrunn) within the Grímsey branch of the Tjörnes Fracture Zone. The southernmost part of the KRISE profile runs along the western edge of the Grímsey shoal parallel to the Eyjafjarðaráll basin.

[11] The KRISE seismic refraction data were collected using the University of Bergen research ship, Håkon Mosby, and the Icelandic coast guard cutter, Ægir. For Profile 1, we used 14 ocean bottom seismometers (OBS) from the University of Hokkaido. The OBSs included both digital and analog instruments with three-component, 4.5 Hz sensors and were spaced approximately 15 km

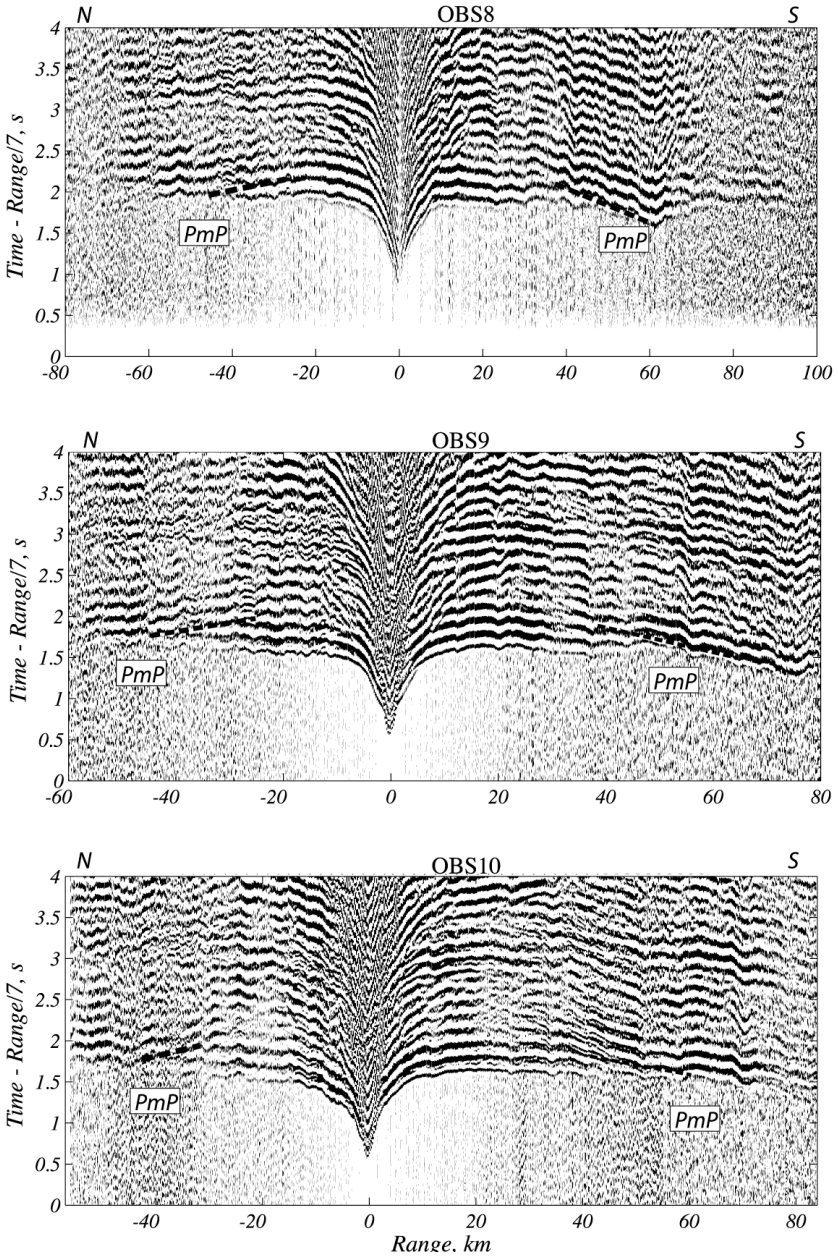

Figure 4c. Record sections for OBS8, OBS9, and OBS10, plotted as in Figure 4a.

apart. OBS3 was not recovered and two instruments had irretrievable data (OBS13 and OBS11). The seismic source was a four-element air gun array with a total capacity of 4800 in^3 (78 l) towed at a depth of 8 m. The shots were spaced every 180 m, corresponding to a shot rate of approximately 70 s. Shot positions were obtained using the shipboard Global Positioning System. Ocean floor and basement reflections were recorded for each shot on a 20-m long minihydrophone streamer (Figure 3).

[12] As the water velocity is poorly known, we develop a grid search method to relocate the OBSs, find the water velocity, and determine timing shifts (Appendix A). The relocated OBS positions, depths, and water velocities are given in Table 1. The OBS depths range from 151 to 915 m. As expected, the average water velocity was low, 1.450 km/s; water velocities in the shallower, warmer water near Iceland are higher 1.465 to 1.470 km/s. On average the stations are shifted along the profile 17 m to the south with a

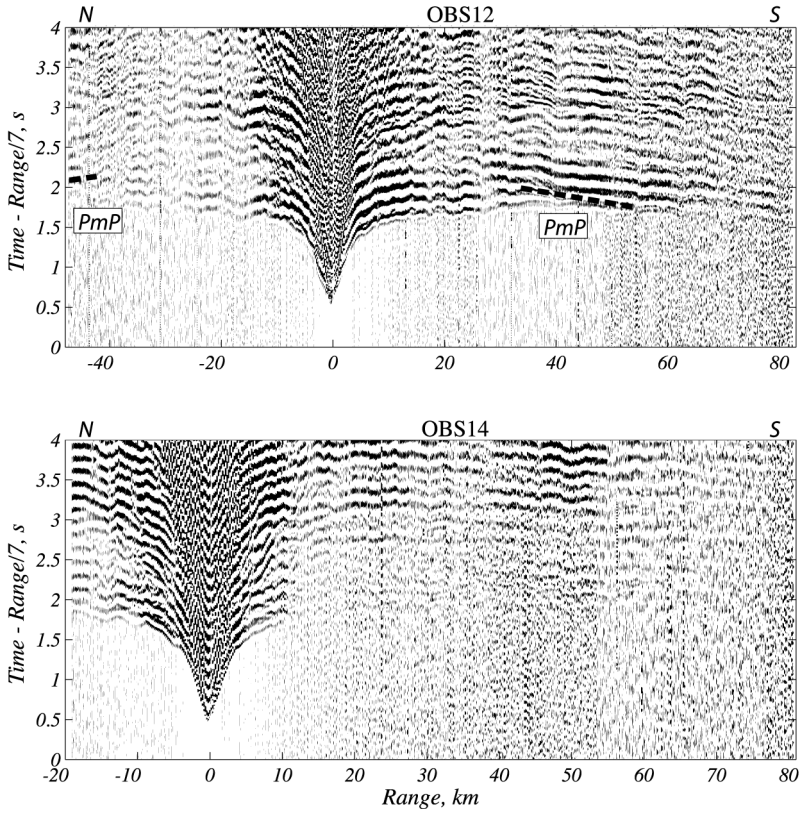

Figure 4d. Record sections for OBS12 and OBS14, plotted as in Figure 4a.

range from 124 m to the south to 109 m to the north. The accuracy of the locations is about 50 m along the profile. The time shift is generally small (−30 to 30 ms) except at OBS 6 and OBS 8 where the time shift is 100 and 300 ms, respectively. This may indicate that these stations were located off the profile by 430 m to 960 m, respectively. The accuracy of the timing is about 18 ms.

4. Data and Seismic Modeling

[13] Record sections for the 11 OBSs used to invert for crustal structure and thickness are shown in Figures 4a–4d. Sea conditions were excellent during the experiment and we recorded good quality data out to ranges of 60 to 100 km. To pick travel times for the *P* and PmP arrivals, the OBS data is band-pass filtered from 3 to 20 Hz. We hand pick 3451 *P* arrivals with a typical uncertainty of 25 ms and 1109 PmP arrivals with a typical uncertainty of 35 ms. Care was taken to only pick PmP arrivals that could not be confused with Pn arrivals. To determine the level to which a model should fit the data, we sum the estimated variances of all the uncertainties in a travel time observation. The largest sources of uncertainty are OBS position, identification of arrival time, and timing error (Tables 1 and 2). The final predicted uncertainty of *P* and PmP arrival times are 31 and 40 ms, respectively.

[14] We invert *P* and PmP arrival times to obtain the two-dimensional *P* wave crustal velocity model and depth to Moho using the method of *Korenaga et al.* [2000]. This method performs a joint refraction and reflection travel time tomography inversion to simultaneously invert for the seismic velocity field and depth of a reflecting interface. The forward problem is solved by a hybrid method using the shortest path [*Moser*, 1991] and the ray-bending method [*Moser et al.*, 1992]. The inverse problem uses a sparse least squares method [*Paige and Saunders*, 1982] to solve a regularized linear system.

[15] The velocity model is parameterized as a sheared mesh hanging from the seafloor topography with horizontal nodes every one km and depth nodes spaced incrementally from 50 m near the seafloor to 1 km at 20 km depth. The Moho is

Table 1. Result of Station Relocations

OBS	Drop Latitude, deg	Drop Longitude, deg	Drop Depth, m	Relocated Latitude, deg	Relocated Longitude, deg	Relocated Depth, m	Dist. Along Profile, km	Shift Along Profile, m	Time Shift, ms	Water Velocity, km/s	Shot Offset, km
1	−18.6103	66.7017	341	−18.6098	66.7028	341	202	−120	10	1.465	0.178
2	−18.5603	66.7987	382	−18.5601	66.7991	382	191	−50	−20	1.465	0.159
4	−18.4533	67.0717	151	−18.4534	67.0714	150	160	40	30	1.470	0.175
5	−18.4005	67.1977	395	−18.4006	67.1974	396	146	30	−30	1.450	0.180
6	−18.3473	67.3227	532	−18.3473	67.3228	532	132	−10	100	1.450	0.183
7	−18.2937	67.4487	548	−18.2941	67.4477	550	118	110	30	1.450	0.182
8	−18.2403	67.5747	798	−18.2401	67.5751	799	104	−40	300	1.450	0.170
9	−18.1863	67.7008	875	−18.1863	67.7009	875	90	−10	0	1.450	0.194
10	−18.1333	67.8257	915	−18.1331	67.8262	913	75	−60	0	1.450	0.181
12	−18.0265	68.0778	827	−18.0262	68.0784	825	47	−70	−30	1.450	0.181
14	−17.9203	68.3288	728	−17.9203	68.3287	728	19	10	10	1.450	0.196

parameterized as a floating reflector with nodes every 2 km with one degree of freedom in the vertical direction. The inversion is regularized with smoothing constraints that are imposed using weighted correlation lengths. For the velocity model we use a depth-dependent horizontal correlation length that increases linearly from 1 km at the seafloor to 16 km at the bottom of the model (20 km below the seafloor), and a vertical correlation length that also increases linearly from 0.1 km at the seafloor to 2 km at the bottom, both weighted by a factor of 700. The correlation length for the depth nodes of the reflector is 9 km, weighted by a factor of 3. Also the depth sensitivity is weighted by a depth kernel weighting parameter (w). Four iterations of the forward and inverse problem are performed for each analysis.

[16] We first invert the crustal refractions, P, to determine the best fitting velocity-depth model for the KRISE area (Figure 5) using a starting velocity-depth model based on the Reykjanes Ridge [*Weir et al.*, 2001]. For the best fit velocity-depth model the root mean squared (RMS) travel time residual for P is 86 ms and χ^2 is 12, where

$$\chi^2 = \frac{1}{N-1}\sum_{i=1}^{N}\left(\frac{t_{i,obs} - t_{i,calc}}{\sigma_i}\right)^2 \quad (1)$$

and $t_{i,obs}$, $t_{i,calc}$, and σ_i are the observed and calculated travel time and standard deviation for the ith of a total of N observations.

[17] Next, we perform a two-dimensional inversion of crustal structure for the P arrivals using the best fit velocity-depth profile as a starting model. Most of the P rays turn within the upper 4–5 km and to avoid artificial velocity perturbations at depth, we damp the velocity perturbations below 4 km depth. For the P arrivals, the two-dimensional inversion has a RMS travel time residual of 36 ms and χ^2 of 2.1.

Table 2. Travel Time Uncertainty

Largest Error Sources	Location Error, m	Timing Error, ms
OBS location and depth	50, 1	6
Timing error	-	18
Picking of first arrivals	-	25
Picking of PmP arrivals	-	35
Total, first arrivals		31
Total, PmP arrivals		40

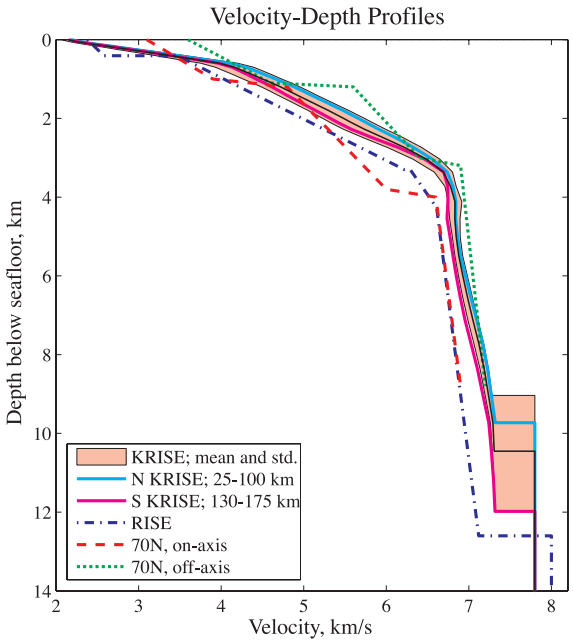

Figure 5. Plot of velocity versus depth showing the mean and standard deviation for the entire KRISE profile (black line and pink region). Also shown are the average velocity-depth profiles for the northern and southern sections of KRISE line 1 (25–100 km, heavy blue line, and 130–175 km, heavy red line, respectively). For comparison we plot the velocity-depth profiles for (1) the RISE line along the Reykjanes Ridge at the same distance from the Iceland plume [*Weir et al.*, 2001] (dash-dot line) and (2) the on- and off-axis velocity profiles farther north at 70°N on the Kolbeinsey Ridge (dashed and dotted lines, respectively) [*Kodaira et al.*, 1997].

[18] Finally, we perform joint inversions of *P* and PmP arrivals for crustal structure and Moho depth. To explore tradeoffs between lower crustal velocity structure and Moho topography and investigate inversion stability, we (1) generate a series of inversions with starting Moho models ranging in depth from 10 to 15 km (both horizontal and sloping down toward Iceland) and depth kernel weighting factors, *w*, varying between 1, 5, and 10 and (2) perform inversions with starting crustal velocity models where ±0.1 km/s and ±0.05 km/s are added to the lower crustal velocities (>4 km depth). Sixteen inversions fit the data equally well (average RMS travel time residual and average χ^2 for both *P* and PmP is 34 ms and 1.5; for *P* is 32 ms and 1.6; and for PmP is 40 ms and 1.0) (Table 3). Our final model for crustal structure and Moho depth is obtained by averaging the result of these 16 models (Figure 6a).

[19] In Appendix B, we investigate the resolution and reliability of our final crustal model by (1) investigating the resolution of the model, (2) exploring the dependence of the recovered structure on the starting model and inversion parameters, (3) inverting synthetic checkerboard-pattern crustal velocity anomalies, and (4) performing synthetic resolution tests for sinusoidal undulations in Moho depth. We find that the resolution of the crustal model depends on the ray coverage, the instrument spacing, and the velocity gradients. We conclude that while the upper crust is best resolved in the southern part of the profile, between 100 and 200 km, the lower crust and Moho are best

Table 3. Fits for Sixteen Equally Fitting Crustal Models

	Initial Moho, km				P and PmP (4560)		P (3451)		PmP (1109)	
Job	N	S	Weight W	l.c. Vel. Pert., km/s	RMS, s	χ^2	RMS, s	χ^2	RMS, s	χ^2
517	10	15	5	0	35	1.5	32	1.6	44	1.2
519	10	15	10	0	35	1.5	32	1.6	44	1.2
520	12	12	5	0	34	1.5	32	1.6	39	1.0
522	12	12	10	0	34	1.5	32	1.6	40	1.0
523	10	10	5	0	34	1.5	32	1.6	40	1.0
524	10	10	1	0	34	1.5	32	1.6	40	1.0
525	10	10	10	0	34	1.5	32	1.6	40	1.0
526	10	12	5	0	34	1.4	32	1.6	39	1.0
527	10	12	1	0	34	1.5	32	1.6	41	1.0
528	10	12	10	0	34	1.5	32	1.6	40	1.0
617	10	15	5	0.1	35	1.5	32	1.6	45	1.2
617_2	10	15	5	−0.1	36	1.5	32	1.6	46	1.3
617_4	10	15	5	−0.05	35	1.5	32	1.6	44	1.2
626	10	12	5	0.1	34	1.5	32	1.6	40	1.0
626_2	10	12	5	−0.1	34	1.5	32	1.6	41	1.0
626_4	10	12	5	0.05	34	1.5	32	1.6	40	1.0

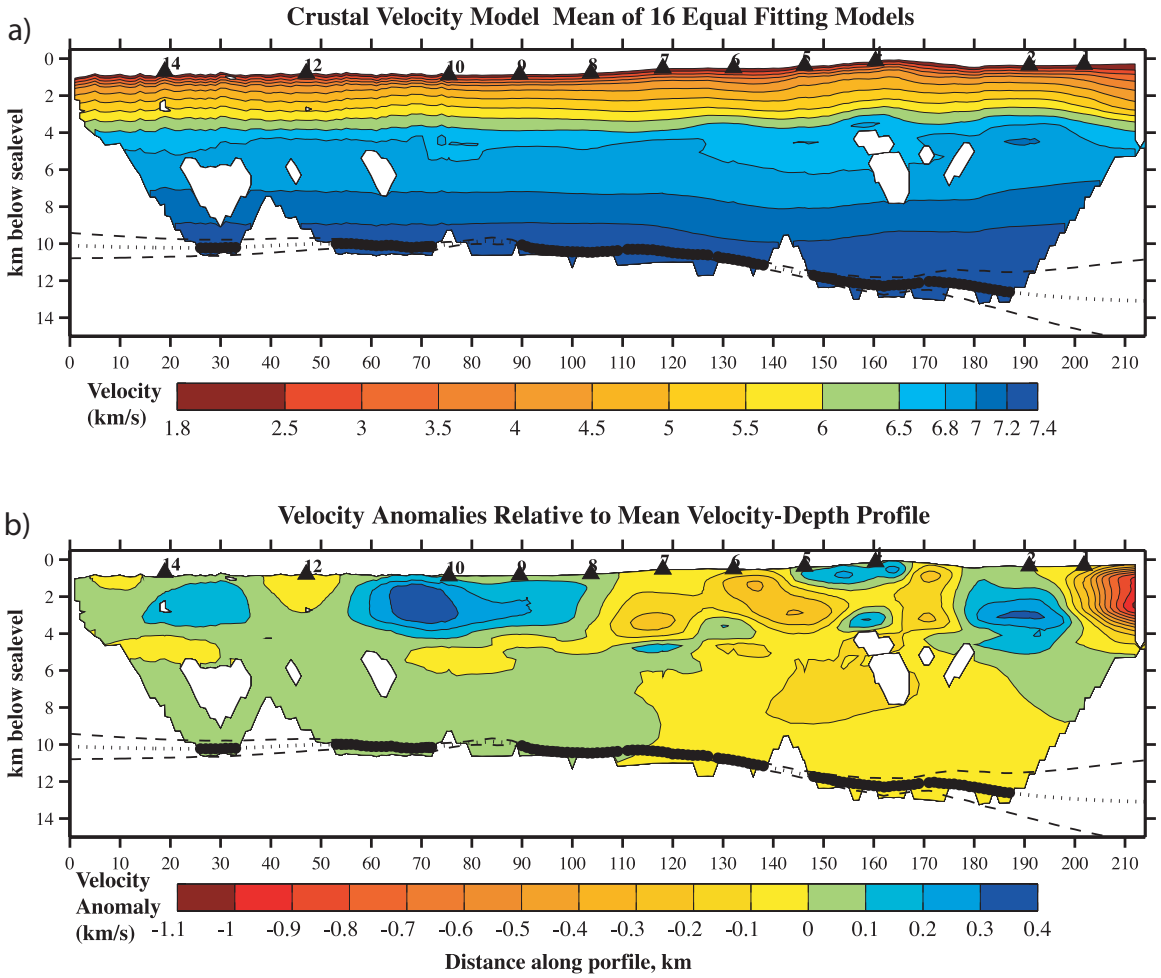

Figure 6. (a) Final crustal velocity model is the mean of the 16 equally fitting models in Table 3. The Moho topography (dotted line) is shown with a heavy line where it is well constrained, and the uncertainty (two standard deviations) is the dashed line. (b) Velocity anomalies relative to the mean velocity-depth profile.

resolved in the central portion of the profile, between 60 and 130 km.

5. Results

[20] We present our best fitting velocity-depth and 2-D seismic crustal models and their uncertainties in this section. We also present the mantle density variations obtained by inverting the gravity data using the crustal structure model and Moho depth.

5.1. Average Velocity-Depth Model

[21] The typical seismic structure of oceanic crust consists of a lower velocity upper crust and a higher velocity, low-gradient lower crust. The upper crust is seismically defined by a low velocity (<2.5–5 km/s) upper layer 2A overlying a higher velocity layer 2B (~5–6 km/s) [*Christeson et al.*, 1994; *Harding et al.*, 1993; *Houtz and Ewing*, 1976; *Vera et al.*, 1990]. The lower crust includes a thick, nearly constant-velocity layer 3 (~6.8 km/s) overlying a layer (mean velocity ~7.4 km/s) thought to be a transition to the underlying mantle [*Houtz and Ewing*, 1976; *Houtz*, 1976]. It is typically believed that seismic layer 2A corresponds to the extrusive section, layer 2B to the sheeted dike section, and layer 3 to isotropic and layered gabbros [*Detrick et al.*, 1994; *Dilek*, 1998; *Talwani et al.*, 1971].

[22] The best fit velocity-depth model for Profile 1 (Figure 5) has a 3.5 km thick layer 2 with an upper low-velocity layer 2A that is 0.7–1 km thick. Lower crustal velocities throughout the region increase with depth from 6.8 km/s at 3.5 km depth

Table 4. Crustal Thickness Along Profile

Mean Latitude, °N	Mean Longitude, °W	Starting Distance, km	Ending Distance, km	Mean Distance, km	Mean Seafloor Depth, m	Mean Crustal Thickness, km	Mean Bathymetry, m	Standard Deviation Crustal Thickness, km
68.2345	−17.9598	26	34	30	824	9.4	880	0.2
67.9412	−18.0848	52	72	62	840	9.3	905	0.1
67.6124	−18.2240	89	110	100	824	9.5	830	0.1
67.4391	−18.2974	110	128	119	569	9.8	550	0.1
67.3103	−18.3527	128	138	134	533	10.4	535	0.1
67.0880	−18.4466	148	170	158	217	11.7	230	0.2
66.9058	−18.5242	170	188	179	359	12.1	365	0.4

to 7.3 km/s at 11 km depth. Comparison of the KRISE velocity depth structure with the Kolbeinsey Ridge north of the Spar offset (between 69°30′N and 70°20′N [*Kodaira et al.*, 1997]) and Reykjanes Ridge south of Iceland (the RISE experiment between 64°N and 62°40′N [*Weir et al.*, 2001]) (Figure 5) shows that the velocity structures are comparable with lower velocities at near-axis profiles (70°N on-axis and RISE). The thickness of the entire layer 2 (2A + 2B) is similar at all locations (3.5–4 km); apparent differences in the thickness of layer 2A may be due to the coarser model parameterization of the earlier studies.

5.2. Upper Crustal Velocities

[23] Our final model for crustal structure and Moho depth is obtained by averaging the result of 16 equally fitting joint inversions of *P* and PmP arrivals (Table 3 and Figure 6a). Crustal velocity anomalies relative to the average velocity-depth function are shown in Figure 6b. Crustal velocity anomalies are concentrated in the upper 4 km of the crust, within the higher velocity gradient layer 2. The checkerboard resolution tests show that the best resolved anomalies lie between distances 100 to 200 km (Figure B2a). In this area, we find regions of low and high velocities with amplitudes ranging from −0.3 km/s to 0.3 km/s and horizontal and vertical wavelengths of 5 to 15 km and 1 to 3 km, respectively.

[24] On the southernmost part of the KRISE profile, south of distance 200 km, upper crustal velocities are unrealistically low, as a decrease in velocities is required by late arrivals south of station 1 (Figure 4a). This may be because sediments thicken very rapidly south of this location toward Iceland; they were not well imaged in the single channel reflection data due to the multiple reverberations generated in the shallow water in this region. It is likely that arrivals at OBS1 are affected by the Eyjafjarðaráll basin, where previous reflection experiments indicate sedimentary thicknesses of up to 4 km [*Gunnarsson*, 1998].

5.3. Crustal Thickness and Lower Crustal Velocities

[25] Crustal thickness changes along the KR are relatively smooth (Table 4, Figures 6 and 7). Crustal thickness north of the Iceland shelf, is approximately uniform, 9.4 ± 0.2 km at distances 25 to 100 km. To the south the water shoals on the Iceland shelf and crustal thickness increases by 2.6 ± 0.5 km, from 9.5 ± 0.1 km to 12.1 ± 0.4 km,

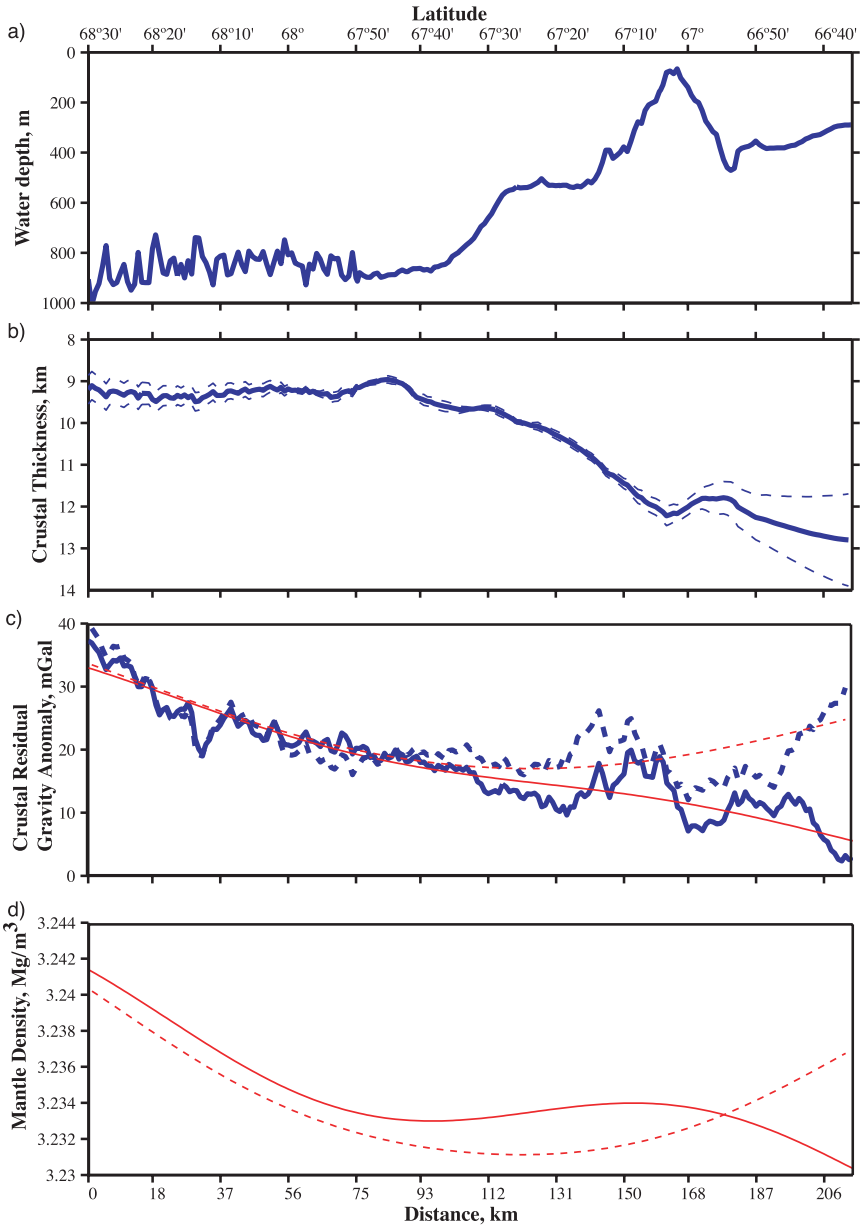

Figure 7. (a) Water depth, (b) crustal thickness, (c) crustal residual gravity anomaly, and (d) mantle density plotted as a function of distance along the KRISE profile. Latitude is labeled at the top of the figure. (c) Crustal residual gravity anomaly (heavy lines) is calculated both by assuming uniform crustal density (solid line) and by calculating crustal densities from crustal velocities (dashed line); see text for discussion. (d) Mantle density anomalies are calculated by downward continuation of the crustal residual gravity anomaly using a compensation depth of 100 km and a band-pass filter from 170 to 1000 km; same line styles as in Figure 7c. Figure 7c also shows the component of the crustal residual gravity anomaly that is accounted for by the mantle densities variations inferred in Figure 7d (thin lines). Note the almost constant crustal thickness and uniform water depths north of the Icelandic shelf, about 67°30′N. This contrasts with the relatively linear increase in crustal thickness and topography south of the shelf toward Iceland. Crustal thickening beneath Stóragrunn is small: 300–500 m.

over 90 km. This increase is more or less linear at a rate of 0.29 km of crust per 10 km distance along the profile. Our profile passed directly over the large volcano Stóragrunn at the junction of the Kolbeinsey Ridge axis with the Grímsey Rift Zone. Beneath Stóragrunn, between 148 and 172 km, the crust thickens slightly, by 0.3 km to 12.2 ± 0.3 km.

[26] The crustal thickening south of the Iceland shelf is accompanied by a decrease in lower crustal

velocities, by 0.07–0.15 km/s between 4 and 10 km depth. At the same time, because the crustal velocities are equal below 10 km depth, the average lower crustal velocity increases as the crust thickens. The most pronounced lower crustal velocity reduction, more than 0.15 km/s, is at about 7 km depth and located beneath Stóragrunn (Figure 6b). Crustal velocities averaged along the northern and southern portions of the profile (25–100 and 130–175 km, respectively) are compared to the mean velocity-depth profile in Figure 5. These differences in lower crustal velocity are resolvable as they are greater than the standard deviation of the velocity (Figure B1b).

5.4. Gravity Inversion and Mantle Density Variations

[27] We use the KRISE seismic crustal thickness and structure to calculate the contribution of the crust to the observed free air anomaly. We remove the effect of the seafloor topography and the crustal density structure and thickness from the free air gravity data to obtain the residual crustal gravity anomaly (Figure 7c). We convert crustal seismic structure to density in two ways. First, we assume that the crust has a uniform density of 2850 Mg/m^3. Second, we calculate crustal densities from the crustal velocities using the relationship of *Carlson and Raskin* [1984] for diabase and gabbros. The baseline mantle density is 3240 Mg/m^3 similar to that determined beneath the Reykjanes Ridge [*Weir et al.*, 2001]. We find that the calculated crustal residual gravity anomaly decreases by about 30 to 40 mGal toward Iceland (Figure 7c).

[28] Variations in the crustal residual gravity anomaly may be attributed to density variations in the mantle. To infer mantle density variations, we downward continue the crustal residual gravity anomalies using the method of *Parker and Huestis* [1974] (as coded by *Korenaga et al.* [2001]). The compensation depth is taken to be 100 km. To stabilize the downward continuation, the smallest wavelength crustal residual gravity anomaly used is 170 km. We infer that mantle densities decrease by about 8 kg/m^3 (0.008 Mg/m^3) toward Iceland (Figure 7d). The predicted mantle density variation accounts for the long-wavelength component of the crustal residual gravity anomalies (Figure 7c). Along the Reykjanes Ridge inferred mantle density variations also decrease toward Iceland together with a increase in crustal thickness: the density variations are of similar wavelength but are twice as large, 0.015 to 0.02 Mg/m^3 [*Weir et al.*, 2001]. In contrast to the patterns in crustal thickness (Figure 7b), the fluctuations in inferred mantle density anomalies along the KR are more pronounced north of the Iceland shelf and the inferred mantle density anomalies are more uniform on the Iceland shelf (Figure 7d).

6. Discussion

6.1. Crustal Velocity Anomalies Along the Kolbeinsey Ridge

[29] In the upper crust, low velocity anomalies (<−0.3 km/s) are found in two regions (Figure 6b). The first low velocity anomaly is beneath a small volcanic cone that is 50 m high and 2.6 km wide and is located at the base of the northern flank of Stóragrunn volcano (130–140 km). The second low velocity anomaly is beneath the southern flank of Stóragrunn (168–177 km) and coincides with the apparent eruption point of a hummocky pillow flow observed in high-resolution bathymetry [*Brandsdóttir et al.*, 2004]. These low velocity anomalies may represent higher porosities (more recent extrusives where cracks have not yet been filled with alteration products) or higher-temperature regions associated with these volcanic features.

[30] In contrast to the low velocities found beneath the south flank and to the north of Stóragrunn volcano, high velocity anomalies (>0.2 km/s) are found in the uppermost crust of the volcano and beneath its northern flank (145–165 km) as well as at crustal depths of 3–4 km directly beneath Stóragrunn (155–162 km) (Figure 6b). Though imaged separately these high velocity anomalies might be part of a single body. The high velocities in the uppermost crust are similar to high velocities found around the caldera at Katla volcano [*Gudmundsson et al.*, 1994] and may be due to the presence of shallow intrusives. However, the mid-crustal high velocity body directly beneath Stóragrunn volcano is significantly smaller than the 7 km high lower crustal dome found beneath the Krafla caldera [*Brandsdóttir et al.*, 1997; *Staples et al.*, 1997]. High velocity domes in the lower crust are typically observed on Iceland beneath both active and extinct volcanoes at the center of volcanic segments [*Brandsdóttir et al.*, 1997; *Menke et al.*, 1998]. These anomalies are believed to consist of cooled, high-density basaltic intrusives such as gabbroic cumulates that form beneath an upper-crustal magma chamber [*Menke et al.*, 1998; *Staples et al.*, 1997]. South of Stóragrunn the northernmost part of the Grímsey shoal

(180–200 km), also appears to be underlain by a high velocity anomaly that may be directly analogous to the lower crustal domes observed on Iceland. This dome may be associated with an older and eroded, extinct system analogous to doming seen in northern Iceland west of the current neovolcanic zone [*Menke et al.*, 1998].

[31] While Icelandic high velocity domes extend up from the lower crust, at Stóragrunn the mid-crustal high velocity body is directly underlain by a broad (25 km wide) low-velocity anomaly in the lower crust (5.5–9 km depth) with amplitude of up to −0.15 km/s. Three local processes may reduce the lower crustal velocity beneath Stóragrunn: (1) the presence of high temperatures and/or melt beneath this active volcano, especially in comparison to the northern portion of the profile where crust has cooled to its current location 7–8 km away from the KR axis; (2) the presence of high porosities throughout the crust due to tectonics at the junction of the KR with the Grímsey Rift Zone; and (3) greater magmatic differentiation due to the off-axis location of Stóragrunn volcano and possible greater complexity in melt delivery from the mantle to the crust than beneath the ridge axis. This last process is less likely as lavas from Stóragrunn have high MgO and are thus appear relatively unevolved. Both of the first two processes may be occurring and further investigation is required to distinguish the contributions of temperature, melt, and porosity to decreasing the lower crustal velocity beneath the Stóragrunn volcano at the junction of the KR with the Grímsey Rift Zone.

6.2. Crustal Thickness Patterns and Melt Flux Along the Kolbeinsey Ridge

[32] North of the Iceland shelf along the KR, the uniform crustal thickness corresponds to a relatively constant melt flux of 0.19 km^2/yr (volume of melt per unit time per length of ridge segment). Along the southern portion of the KR on the Iceland shelf, crustal thickness indicates that melt flux increases uniformly toward Iceland to a value of 0.24 km^2/yr, an increase by a factor of 1.26. The crustal thickness pattern is mirrored in relatively constant $Na_{8.0}$ values on the northern section of the profile and a proportional decrease in $Na_{8.0}$ along the southern part of the KR (C. Devey, personal communication, 2005). Trace elements show the same pattern (constant values in the north and a linear trend to the south) in ε_{Hf} and ε_{Nd} values along the KR [*Blichert-Toft et al.*, 2005]. Crustal thickness and major element chemistry support a melt flux increase by 25% along the southern portion of the KR on the Iceland shelf. (This is reflected in the elevated morphology of the ridge axis south of 67°15′N [*Brandsdóttir et al.*, 2004]).

[33] Crustal thickness everywhere along the KR is greater than for typical oceanic crust at the Mid-Atlantic Ridge (MAR): 9.4 to 12.1 km compared to 5.5 ± 0.4 km [*Hooft et al.*, 2000], respectively. This represents a melt flux of 0.19 to 0.24 km^2/yr compared to 0.11 km^2/yr for typical MAR crust. Relative to the MAR, melt flux at the KR is elevated by a factor of 1.7 to 2.2 (on the northern and southern portions of profile 1, respectively). Melt flux along the KRISE profile has a characteristic pattern. North of the Iceland shelf, melt flux is relatively constant while also elevated compared to typical MAR. Nearer Iceland, on the Iceland shelf, there is an additional steady increase in melt flux toward Iceland.

[34] The greater melt flux on the KR relative to the MAR is accompanied by a change in how melt is delivered to the crust. Crustal thickness variations along the KR and RR are relatively smooth (Figure 7 and *Weir et al.* [2001]) and we do not observe crustal thickness undulations similar to those associated with segmentation of the MAR, where crustal thickness changes of ∼1–3 km are associated with ridge segments 50–90 km long [*Hooft et al.*, 2000]. It is possible that plumbing processes resulting from the more pronounced segmentation of the MAR axis focus mantle melt laterally resulting in smaller wavelength crustal thickness variations [e.g., *Hooft et al.*, 2000]. In contrast, the influence of the Iceland hot spot appears to cause gradual variations in crustal thickness and melt flux over long distances (several hundred kms). This difference may also be related to lower crustal temperature, the lower crust in the vicinity of Iceland being sufficiently hot to allow ductile lower crustal flow on a larger scale [*Bell and Buck*, 1992]. Alternatively, the influence of the plume on the lithosphere may cause continual ridge axis reorganizations [*Appelgate*, 1997] such that segmentation in mantle upwelling is not well established. Note that further from the Iceland hot spot, north of the Spar offset, crustal thickness at the KR axis appears to be more variable [*Kodaira et al.*, 1997].

6.3. Mantle Temperature Variations and Active Upwelling Along the Kolbeinsey Ridge

[35] The observed changes in crustal thickness, inferred mantle density anomalies, and major ele-

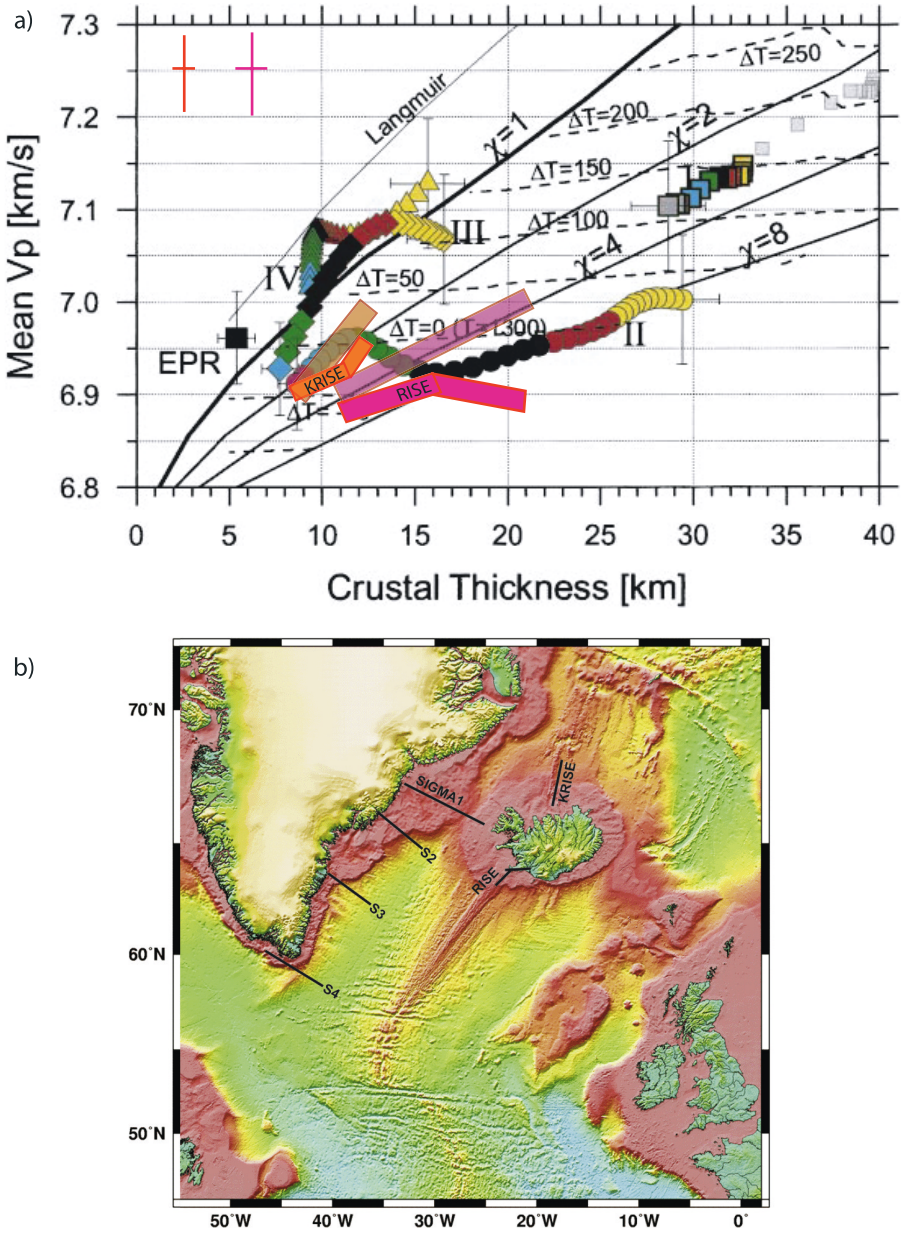

Figure 8. (a) Mean crustal velocity and crustal thickness data for KRISE (orange) and RISE (pink) compared with data from four profiles off the Greenland coast, SIGMA (reproduced from *Holbrook et al.* [2001] with permission from Elsevier). Mean crustal velocities for KRISE and RISE are determined as by *Holbrook et al.* [2001] for two crustal thermal models, one with 750°C at the Moho (solid boxes) and the other with 800°C fixed at 10 km depth (transparent boxes); see text. Typical errors for KRISE and RISE are shown in the upper left corner. Predictions of mean crustal velocity and crustal thickness systematics are shown for two melting models, *Langmuir et al.* [1992] (thin line) and the *McKenzie and Bickle* [1988] model, assuming passive upwelling (bold line) and active upwelling ratios (X) of 2, 4, and 8. Dashed lines represent mantle potential temperature for the *McKenzie and Bickle* [1988] model. OC represents the calculated mean crustal velocity of oceanic crust near the East Pacific Rise [*Holbrook et al.*, 2001]. (b) Map showing the locations of the seismic profiles (bathymetry derived from satellite altimetry [*Smith and Sandwell*, 1997]).

ment chemistry are consistent with mantle temperature variations. Assuming passive upwelling, we can infer variations in mantle potential temperature from crustal thickness changes [*White*, 1993]. This results in a mantle potential temperature along the northern portion of the KR that is elevated by about

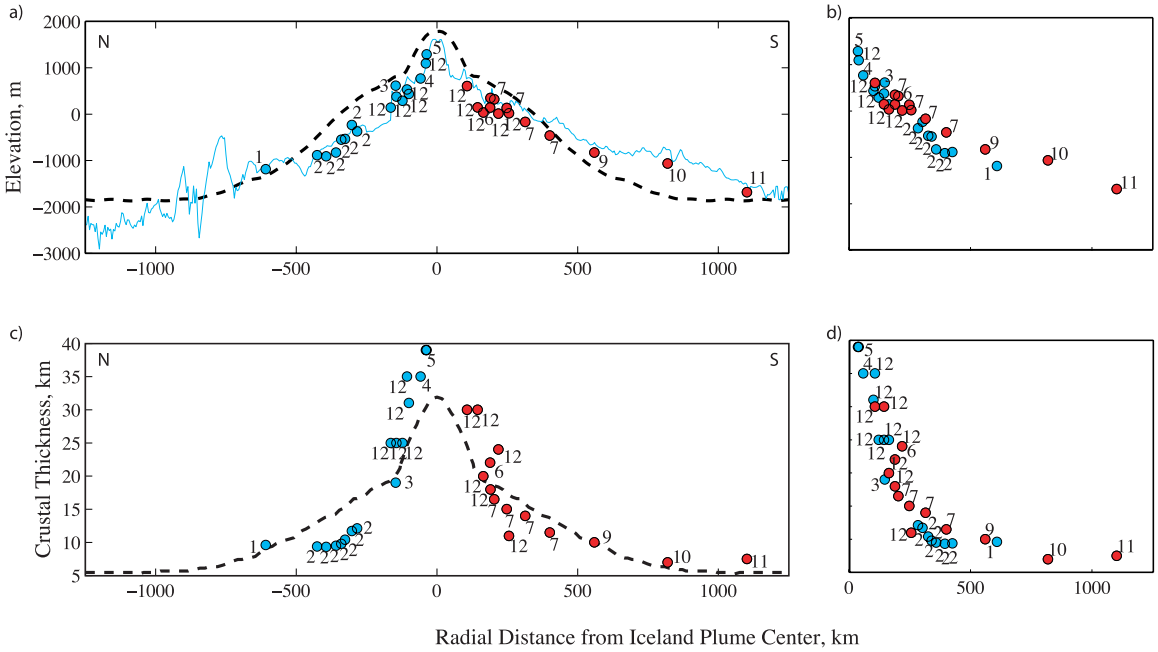

Figure 9. Compilation of crustal thickness measurements (circles) around Iceland compared to the predictions from the model of [*Ito et al.*, 1999] (dashed line). Seismic measurements of crustal thickness are labeled as follows: (1) *Kodaira et al.* [1997]; (2) this paper; (3) *Brandsdóttir et al.* [1997]; (4) *Staples et al.* [1997]; (5) *Darbyshire et al.* [1998]; (6) *Bjarnason et al.* [1993]; (7) *Weir et al.* [2001]; (9) *Smallwood and White* [1998]; (10) *Bunch and Kennett* [1980]; (11) *Navin et al.* [1998], (12) *Menke* [1999]. (a and b) Elevation (thin line) and (c and d) crustal thickness plotted as a function of radial distance from the Iceland plume center. The right panels show the observations from the northern and southern spreading centers overlaid (light and dark gray circles, respectively). Note the north-south asymmetry with thinner crust and deeper spreading centers along the Kolbeinsey Ridge compared to the Reykjanes Ridge.

55°C compared to typical MAR (crustal thickness of 9.4 versus. 5.5 km). South of the Iceland shelf mantle potential temperature increases an additional 40°C toward Iceland (crustal thickness of 12.1 versus. 9.4 km) or 95°C relative to typical MAR. This corresponds to a gradient in mantle potential temperature of 4.4°C per 10 km over the Iceland shelf.

[36] Mantle temperature changes will result in mantle density changes, however mantle density variations are also caused by mantle depletion and/or melt retention [*Ito et al.*, 1996]. If the variations in mantle density anomalies inferred from gravity (Figure 7d) are solely due to thermal expansion (coefficient of thermal expansion 3.4×10^{-5} K^{-1}) then along the KR the inferred mantle temperature variation is 70°C. The inferred mantle temperature variations are smaller if mantle depletion and/or melt retention effects are included; for example, using a mantle depletion of 2%, gives an inferred mantle density variation consistent with that inferred from crustal thickness, 40°C. However, we note that in contrast to the patterns in crustal thickness (Figure 7b), the decrease in mantle density anomaly is most pronounced north of the Iceland shelf and more constant along the Iceland shelf (Figure 7d).

[37] Increased mantle temperatures and active mantle upwelling are two related processes that affect average crustal velocities and crustal thickness [e.g., *Holbrook et al.*, 2001]. To assess the role of temperature and active versus passive upwelling, we plot mean crustal velocity as a function of crustal thickness (Figure 8). We follow the approach of *Holbrook et al.* [2001] and calculate the mean crustal velocity by correcting to 600 MPa and 400°C (pressure correction 0.00022 km/s/MPa and temperature correction −0.0005 km/s/°C). For the geotherm, we assume 10°C at the seafloor and explore two models for crustal thermal structure one with 750°C at the Moho and the other with 800°C fixed at 10 km depth. To avoid velocities that are affected by alteration or porosity and that are unrepresentative of bulk composition, we replace velocities less than 6.85 km/s with 6.85 km/s before applying temperature and pressure correc-

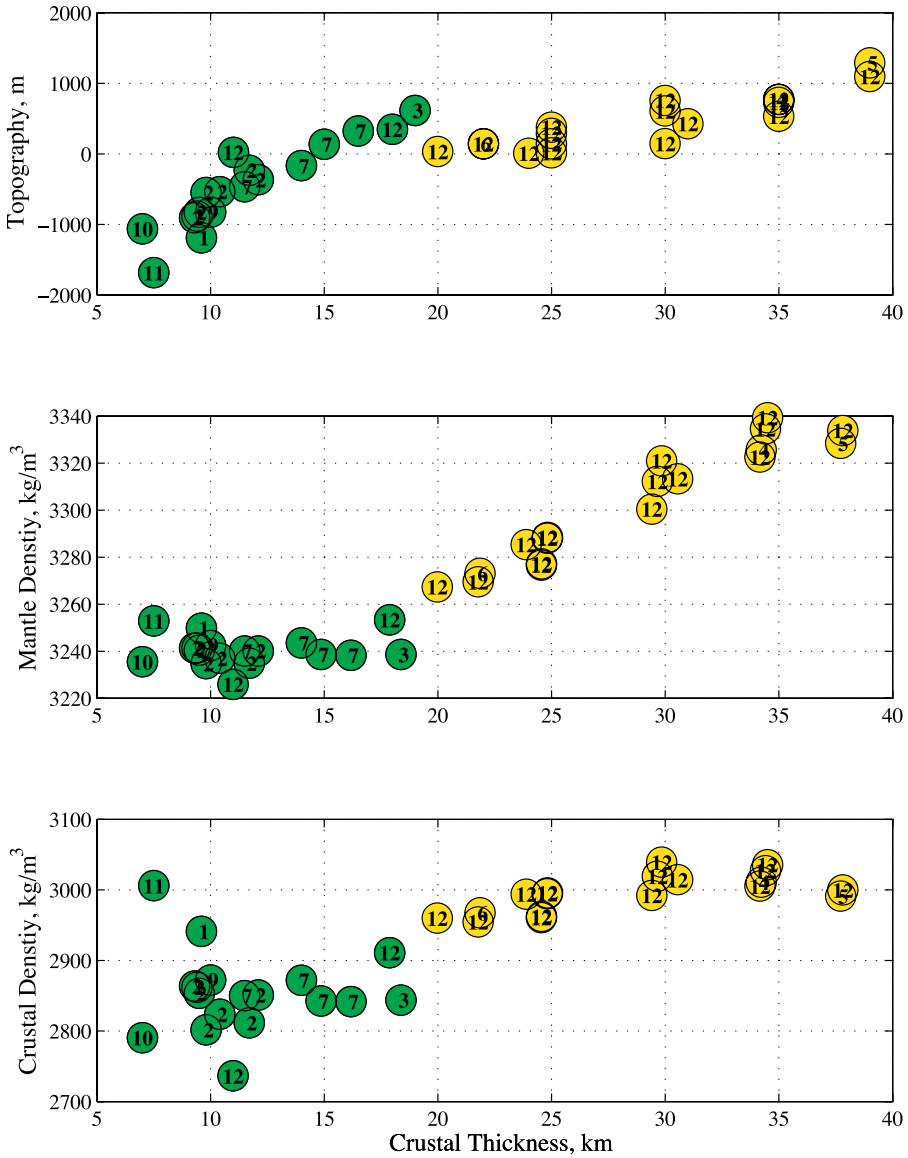

Figure 10. Compensation of topography by crustal thickness; observations labeled as in Figure 9. (a) Elevation as a function of crustal thickness. A linear trend is expected for isostatic compensation with uniform densities for the crust and mantle. Note the relatively low elevation for central Iceland where crustal thickness is great than 20 km (lighter gray circles). (b) Predicted mantle density variations for isostasy with constant crustal density (2850 kg/m^3) and a compensation depth of 100 km. (c) Predicted crustal densities for isostasy with constant mantle density (3240 kg/m^3) and a compensation depth of 100 km.

tions. For the thermal model with temperature fixed at 10 km depth, the mean crustal velocity increases more rapidly as the crust thickens resulting in a greater change in mantle potential temperature along the KRISE profile compared to the model with temperature fixed at the Moho (Figure 8, transparent and solid boxes, respectively). Both thermal models also depend on the value of the bottom isotherm; a hotter geotherm results in a greater thermal correction and a higher mean crustal velocity. This then implies somewhat higher mantle potential temperatures and a lesser component of active upwelling: a 100°C increase in the bottom isotherm corresponds to a change in mantle potential temperature of about 20°C and a change in active upwelling ratio, X, of −0.5.

[38] The choice of crustal thermal model affects the calculated mean crustal velocity, however, the general patterns remain similar. The KRISE profile lies within the field of active upwelling with a potential mantle temperature around 1250°–

1280°C (Figure 8). The mean crustal velocity increases as the crust thickens, consistent with increasing mantle temperatures toward Iceland (by ~50°–90°C) and there is some component of active upwelling (active upwelling ratio, $X \approx 1.5$–2). The KRISE profile lies in the same region of Figure 8 as the Greenland margin profile that is located at a similar distance from the Iceland plume, SIGMA II. This implies that mantle upwelling occurred under similar mantle conditions in these two locations.

[39] The magnitude of the mantle potential temperature variations inferred from crustal thickness variations is similar to that predicted by *Ito et al.*'s [1999] geodynamic model for the Iceland plume that includes mantle dehydration. That model predicts a temperature change of about 75°C at about 100 km depth between 300 and 500 km along the spreading center. This corresponds to a gradient of about 4°C per 10 km. This is similar to the gradient that we infer from crustal thickness patterns on the Iceland shelf.

6.4. Isostatic Support of Topography Around Iceland

[40] Our crustal thickness observations along the KR provide a more complete picture of melt flux at the spreading centers around Iceland and fill a critical gap along the spreading center north of Iceland. We compile crustal thickness and elevation observations (Figure 9) to examine whether support of the topography of the spreading centers about Iceland is isostatic or requires a dynamic component. Figure 10a shows topography from the Iceland neovolcanic zone and adjacent spreading centers as a function of crustal thickness. The most noticeable feature of Figure 10a is that offshore and at Krafla the ratio of topography to crustal thickness is constant, but for central Iceland the topography is low given the large crustal thickness. Along the RR and KR, and at Krafla, topography depends directly on crustal thickness; this indicates that these areas are isostatically compensated and that the different elevation is due to differences in crustal thickness. Using a crustal density of 2850 kg/m^3, water density of 1000 kg/m^3, and compensation depth of 100 km, the linear trend is fit with a mantle density of 3240 kg/m^3. This value of mantle density is similar to that determined for the northern RR (3220 to 3240 kg/m^3 [*Weir et al.*, 2001]). Thus, throughout the oceanic and near coastal parts of the Iceland-Mid-Atlantic Ridge system, topography and crustal thickness are consistent with isostatic support for normal crustal and mantle densities.

[41] The center of Iceland contrasts with the area offshore and at Krafla in having low topography in spite of the large crustal thickness; this has been previously noted by other researchers [*Gudmundsson*, 2003; *Kaban et al.*, 2002; *Menke*, 1999]. Beneath central Iceland, the low elevation can be supported isostatically by a small density contrast across the Moho [*Gudmundsson*, 2003; *Kaban et al.*, 2002; *Menke*, 1999]. Dynamic support of the low topography would require negative pressures beneath Iceland, which is unlikely given the presence of mantle upwelling. To isostatically support the topography crustal and/or mantle densities must vary along the rift zone to the center of the Iceland hot spot.

[42] We calculate the changes in either mantle or crustal density that could isostatically support the observed topography for a compensation depth of 100 km (Figures 10b and 10c). In the case of constant crustal density (2850 kg/m^3), isostatic support requires a large increase in mantle densities beneath Iceland, from 3230–3250 kg/m^3 to 3320–3340 kg/m^3 (Figure 10b). However, mantle densities are actually somewhat reduced beneath central Iceland and the neovolcanic zones [*Darbyshire et al.*, 2000] and we rule out this option.

[43] We then consider isostatic support for a constant mantle density (3240 kg/m^3) and changes in average crustal density (Figure 10c). This model requires normal crustal densities of 2800–2900 kg/m^3 along the offshore spreading centers and beneath Krafla and greater crustal densities beneath central Iceland (2960 kg/m^3 to 3040 kg/m^3). Note that when the geophysically observed reduction in mantle densities beneath Iceland is taken into account [*Darbyshire et al.*, 1998], greater crustal densities are required. While we compute average crustal density, our results confirm the conclusions of *Kaban et al.* [2002] and *Gudmundsson* [2003] that the lower crust beneath Iceland must be considerably denser than that beneath the adjacent ridges. The inferred high-density lower crust is consistent with low attenuation and normal Vp/Vs ratios observed in the lower Icelandic crust [*Darbyshire et al.*, 1998; *Menke et al.*, 1996; *Menke and Levin*, 1994; *Olafsson et al.*, 1998].

[44] The change in the slope of topography as a function of crustal thickness appears to occur when the crustal thickness is greater than about 20 km (Figure 10a) suggesting a relationship between

high melt flux and/or thickened crust and elevated crustal density. *Gudmundsson* [2003] suggests several processes that might increase crustal density: (1) olivine enrichment due to high degree melting beneath Iceland, (2) iron enrichment beneath Iceland due to wet melting and/or iron enrichment in the Iceland plume source, and (3) ecolgite phase transformations (from plagioclase to garnet) that may occur for crustal thicknesses greater than about 25 km. Higher density lower crust (close to that of the mantle) could lead to gravitational instability of the lower Icelandic crust [*Jull and Kelemen*, 2001] and possibly detachment and foundering. We suggest that periodic detachment events might result in subsequent depressurization and melting pulses. This may be an alternative mechanism to generate temporal variations in the flux of the Iceland plume that could explain the V-shaped ridges along the RR.

6.5. Asymmetric Plume-Ridge Interaction North and South of Iceland

[45] Our crustal thickness observations fill a critical gap along the KR north of Iceland and we assess whether or not melt flux at the spreading centers is asymmetric, as has been inferred from bathymetry and geochemistry. Figure 9 compiles crustal thickness and topography observations as a function of radial distance from the center of the Iceland hot spot. At radial distances from the Iceland hot spot center of 200 to 500 km, the crust is 2.0 to 2.5 km thinner to the north along the KR than to the south along the RR (Figure 9d). The center of the Iceland hot spot is assumed to lie beneath northeastern Vatnajökull at 17.3°W, 64.4°N. We find that shifting the location of the hot spot center does not result in greater symmetry of crustal thickness and topography at the spreading centers about Iceland. The difference in crustal thickness between the KR and RR corresponds to an increase in melt flux of about 20% at the RR relative to the KR.

[46] To compare the role of mantle temperatures and active mantle upwelling north and south of Iceland, we apply the same velocity and temperature corrections that were used above to onshore and offshore seismic profiles near the RR (the RISE profiles A and B [*Weir et al.*, 2001]). While the KRISE seismic data were inverted using the same methods as the SIGMA profiles, the RISE data sampled the crust more coarsely and were inverted using different methods [*Weir et al.*, 2001]; thus the comparison of the RISE profile must be made cautiously. Both the KRISE and RISE profiles lie within the field of active upwelling at a range of mantle potential temperatures between 1230°C and 1280°C (Figure 8). The use of two different crustal thermal structures in correcting crustal velocities results in the most pronounced differences for the RR mean crustal velocities. The model with temperature fixed at 10 km depth generates a more consistent increase in mantle temperature toward Iceland, 80–90°C versus no clear increase for the model with temperature fixed at the Moho. In addition, for this thermal correction the RR data lie consistently along the curve for $X = 4$. In spite of these variations, the differences in upwelling pattern between the KR and RR are the same for all thermal models used; the average crustal velocities are higher along the KR than along the RR consistent with greater degree of active upwelling south than north of Iceland ($X \approx 4$ to 8 versus $X \approx 1.5$–2).

[47] The asymmetry in observed melt flux and inferred mantle upwelling mode supports the asymmetry in plume influence north and south of Iceland deduced from axial topography and geochemistry. Elevation of the neovolcanic zone north and south of Iceland is notably asymmetric and between 200 and 500 km from the center of the Iceland hot spot the ridge axis is 200–500 m deeper along the KR than along the RR (Figures 9a and 9b). While we do not image the patterns of upper mantle flow and how they differ north and south of Iceland, we note that moving north from the Iceland plume along the Kolbeinsey Ridge crustal thickness decreases linearly followed by constant, though elevated, crustal thickness. This pattern is very similar to the patterns of both geochemical enrichment (e.g., ε_{Hf} and ε_{Nd}) and the extent of melting, as indicated by $Na_{8.0}$ values (C. Devey pers. comm.). The asymmetry in crustal thickness between the KR and RR (Figures 9c and 9d) is also mirrored in the geochemical enrichment halo which extends 5° along the RR and 1° along the KR [*Blichert-Toft et al.*, 2005]. The geochemical enrichment may be due to deep melting and/or a plume component of melting associated with the Iceland hot spot.

[48] The similar patterns in crustal thickness and geochemical enrichment imply that the Iceland hot spot is influencing mantle melting in two ways. One that has a broad spatial extent and increases melt production gradually yet has limited geochemical enrichment. The other has a more limited spatial extent but has a more pronounced effect on melt production and geochemical enrichment and

is notably asymmetric about Iceland declining more rapidly to the north along the Kolbeinsey Ridge than to the south along the Reykjanes Ridge. The broad region of enhanced melting with limited geochemical enrichment could be due to thermal or viscous entrainment of ambient mantle by the plume or due to secondary convection that is modulated by the nearby continental roots. If the geochemical enrichment is produced by deep mantle melting [e.g., *Ito and Mahoney*, 2005], then the deep melting is spatially limited about Iceland and asymmetric. From the thickness and average velocity of the crust, it also appears that the deep geochemically enriched mantle upwelling is associated with a greater active component of upwelling along the RR than the KR.

[49] The inference of deeper melting along the RR than the KR is not consistent with models of asymmetric Iceland plume-ridge interaction in which the mantle plume spreads at deeper depths to the north than to the south [*Mertz et al.*, 1991; *Schilling*, 1999]; or with models where plume outflow occurs in the asthenosphere and is impeded by lithospheric offsets or other high viscosity boundaries [*Georgen and Lin*, 2003; *Yale and Phipps Morgan*, 1998]. In the first model, we would expect a greater chemical enrichment north rather than south of Iceland due deeper mantle melting beneath the KR. In the second model, we expect no difference in geochemical enrichment north and south of Iceland as all plume outflow occurs at the same depth in the asthenospheric channel in the shallower mantle. On the other hand, the observed asymmetry in geochemical enrichment about Iceland may be due to a plume that is tilted from south to north in the upper mantle as suggested by *Shen et al.* [2002]. The proximity of the deeper part of the plume conduit to the RR might cause preferential deep melting of the enriched mantle plume beneath the RR relative to the KR giving rise to the observed asymmetry in geochemical enrichment about Iceland. In this case, spreading of the plume at shallower depths in the asthenosphere might give rise to the broad region of enhanced melting and limited geochemical enrichment.

7. Summary

[50] Our results quantify the influence of the Iceland hot spot on melt flux at the spreading center north of Iceland. North of the Iceland shelf, crustal thickness is relatively constant over 75 km, 9.4 ± 0.2 km. Along the southern portion of the Kolbeinsey Ridge on the Iceland shelf, crustal thickness increases from 9.5 ± 0.1 km to 12.1 ± 0.4 km over 90 km. We infer that these changes in crustal thickness are accompanied by changes in mantle temperature of 40° to 50°C. Topography and crustal thickness patterns at the spreading centers around Iceland are consistent with isostatic support of topography. We infer that beneath central Iceland the lower crust is considerably denser than that beneath the adjacent ridges and suggest that periodic detachment events could result in subsequent depressurization and melting pulses; possibly causing temporal variations in Iceland plume flux and generating the V-shaped ridges along the RR.

[51] Crustal thickness along the Kolbeinsey Ridge is about 2–2.5 km less than at the Reykjanes Ridge. In this paper, we confirm that there is an asymmetry in plume-ridge interaction north and south of Iceland; the increased crustal thickness and melt flux as well as geochemical enrichment covers considerably shorter distances along the Kolbeinsey Ridge than along the Reykjanes Ridge. Average lower crustal velocities are also slightly higher along the Kolbeinsey Ridge consistent with lower degree of active upwelling than along the Reykjanes Ridge.

[52] Crustal thickness and geochemical patterns suggest that the Iceland hot spot influences mantle melting in two ways. One that has a broad spatial extent and increases melt production gradually yet has limited geochemical enrichment, possibly as a result of shallow melting enhanced by plume outflow in the asthenosphere, thermal or viscous entrainment of ambient mantle, or secondary convection modulated by the nearby continents. The other may be due to deep melting and has a more pronounced effect on melt production and geochemical enrichment but has a more limited spatial extent and is notably asymmetric about Iceland declining more rapidly to the north along the Kolbeinsey Ridge than to the south along the Reykjanes Ridge. The observed asymmetry of the spreading centers about Iceland may be due to a plume that is tilted south to north in the upper mantle [*Shen et al.*, 2002] causing preferential deep melting of enriched material beneath the Reykjanes Ridge.

Appendix A: OBS Relocation and Timing Corrections

[53] To locate each OBS accurately and find any timing errors, we use the seismic energy that travels directly through the water column to the

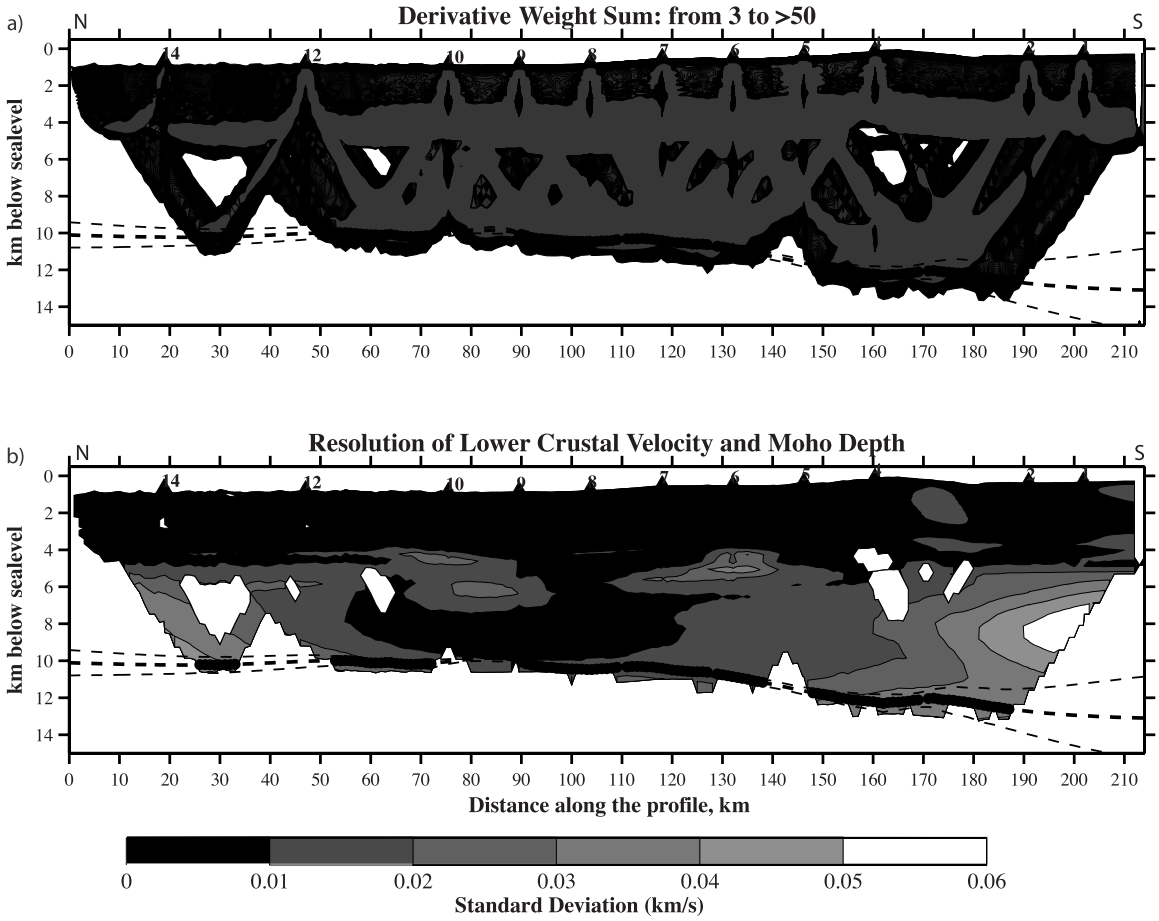

Figure B1. (a) Mean derivative weight sum for the 16 equally fitting models in Table 3. Lighter gray is for values greater than 50. Note the dense ray coverage at the base of layer 2 and through the lower crust and Moho between 50 and 180 km along the profile. (b) Resolution of lower crustal velocity as measured by the standard deviation of the models in Table 3. Note the good resolution in the upper crust (<4 km) and in the lower crust (between 50 and 160 km along the profile); this is consistent with the ray coverage as indicated by the derivative weight sum. Moho topography shown as in Figure 6.

OBS. This direct water wave arrival was picked for each station out to ranges of 10 km. Accurate locations for ocean bottom seismometers are frequently determined using the method of *Creager and Dorman* [1982]; however, the water column velocity structure is poorly known during our experiment. We develop a grid search method to determine the best water velocity, and location for each station. Relatively low water velocities are expected since the water temperatures in this area in June typically range from 3°C to −0.5°C between 0 and 500 m water depth, respectively (http://www.hafro.is/Sjora/Hydrography). We first solve for a shot numbering offset of one between the shot file and the headers of the SEGY seismic data files. In relocating the OBSs we assume that they are not significantly offset perpendicular to the profile and that, around each station, an average velocity for the water column is sufficiently accurate. For a given water velocity and station depth we calculate the offset in station location at every shot from the water wave arrival time and shot location. To solve for the water velocity and station offset, we iterate over a range of water velocities to obtain the most consistent station offset for all the shots (i.e., for all ranges). At some stations there remains a discrepancy in predicted water travel time north and south of the station; this is due to timing errors and/or mislocation of the station perpendicular to the profile. We solve for this as a static time shift.

Appendix B: Model Resolution

[54] To investigate the resolution and reliability of our final crustal model, we use several approaches:

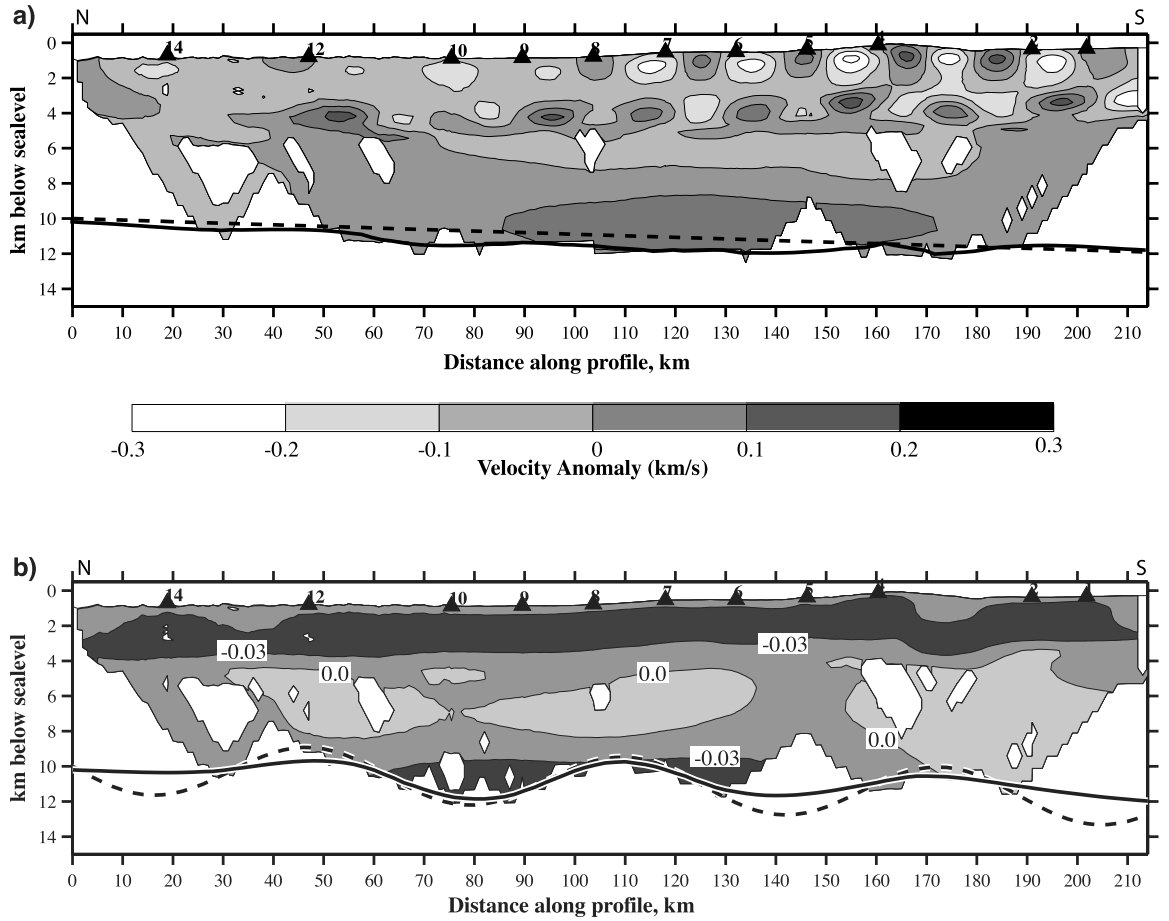

Figure B2. (a) Anomalies recovered during a checkerboard resolution test: 5% anomalies with 20 km horizontal wavelength and 5 km vertical wavelength superimposed on the mean velocity-depth model. Input Moho is linear from 10 to 12 km, north to south (dashed line), and recovered Moho is the solid line. (b) Moho topography recovered (solid line) during a synthetic sinusoidal Moho resolution test: 1.5 km amplitude and 60 km wavelength superimposed on a Moho that slopes from 10 to 12 km from north to south (dashed line). See Appendix B for discussion.

(1) investigate the resolution of the model, (2) explore the dependence of the recovered structure on the starting model and inversion parameters, (3) invert synthetic checkerboard-pattern crustal velocity anomalies, and (4) perform synthetic resolution tests for sinusoidal undulations in Moho depth.

[55] The resolution of the velocity model can be approximated by the derivative weight sum (DWS), which is a weighted sum of the length of ray paths that influence a model parameter [*Toomey et al.*, 1990]. The mean DWS of the 16 best fitting models (Figure B1a) shows high ray coverage and good resolution at the base of the upper crust everywhere and the entire crustal structure is well-resolved in the central portion of the profile, 55 to 130 km.

[56] The standard deviation of the mean of the 16 best fitting models described in the text (Table 3) represents the uncertainty in crustal structure and thickness due to the trade-off between lower crustal velocity and Moho depth (Figure B1b). Two standard deviations of Moho depth ranges from 0.2 to 0.6 km while 2 standard deviations of crustal velocity ranges from <0.01 km/s to >0.05 km/s. These uncertainties are less than the resolved variations in crustal thickness and velocity discussed in the text. The central portion of the profile has high DWS (Figure B1a) and corresponds to the region where the crustal model is not strongly affected by the starting model or inversion parameters (i.e., the standard deviations of velocity and Moho depth are small).

[57] The ability to recover crustal velocity perturbations is assessed by performing inversions of

synthetic travel times calculated for checkerboard velocity patterns (5% velocity anomalies with a 20 km horizontal wavelength and 5 km vertical wavelength) superimposed on the mean velocity-depth profile. Gaussian noise with a standard deviation of 25 msec is added to the synthetic travel times and we use a Moho that increases in depth linearly from 10 to 12 km. Velocity perturbations are well recovered in the upper crust (<4 km) (Figure B2a). The inversion method tends to under-resolve the amplitude of velocity anomalies, which represent an average imposed by the smoothing constraints. Dense station spacing allows shallow crustal perturbations (<2 km depth) to be well recovered along the southern part of the profile (<100 km). Along the northern part of the profile, instrument failure resulted in wider instrument spacing and therefore velocity perturbations are less well recovered. At these wavelengths, velocity perturbations were not recovered in the lower crust. However, the inversion has more sensitivity to positive velocity anomalies than negative anomalies in the lower crust. This results in the reconstruction of a broad region of positive velocity anomaly at 8–10 km depth between 80 and 170 km along the profile. As a consequence the Moho is reconstructed up to 500 m deeper than in the input model.

[58] Moho resolution tests are made for sinusoidal crustal thickness variations with 1.5 km amplitude and 60 km wavelength superimposed on a Moho that slopes from 10 to 12 km depth from north to south (Figure B2b). Gaussian noise with 40 msec standard deviation is added to the synthetic travel times and the mean velocity-depth function is used for the crustal velocities. Along the best-resolved central portion of the profile, 60 and 130 km, undulations in crustal thickness are well recovered; the spatial scale of Moho topography is recovered, the amplitude of the crustal thickness variations are slightly damped, and mapping into lower crustal velocity perturbations is minimal; where crustal thickness increases, velocity anomalies of −0.03 km/s in the lower crust reduced the maximum recovered amplitude by less than 300 m. Along less well-resolved parts of the profile where there are Moho reflections, Moho topography is recovered to within 0.5 km.

[59] The exploration of DWS, inversion parameters and velocity-depth trade-offs, checkerboard tests, and Moho perturbation tests all show that the resolution of the crustal model depends on the ray coverage, the instrument spacing and the velocity gradients. We conclude that while the upper crust is best resolved in the southern part of the profile, between 100 and 200 km, the lower crust and Moho are best resolved in the central portion of the profile, between 60 and 130 km.

Acknowledgments

[60] We thank the crew of the Norwegian research ship, Håkon Mosby, and of the Icelandic coast guard cutter, Ægir, and Andrew Barclay, Oistein Aanensen, Tomoki Watanabe, Tadashi Yamashina, Tetsuo Takanami, and the KRISE Fieldwork Team for their role in collecting the data. We thank two anonymous reviewers for their constructive reviews. This work was funded by the Iceland Science Foundation, NSF grant OCE-9911243, and the University of Iceland Research Fund. We received ship time support from the Icelandic Coast Guard and the University of Bergen.

References

Allen, R. M., et al. (1999), The thin hot plume beneath Iceland, *Geophys. J. Int.*, *137*, 51–63.

Appelgate, B. (1997), Modes of axial reorganization on a slow-spreading ridge: The structural evolution of Kolbeinsey ridge since 10 Ma, *Geology*, *25*, 431–434.

Bell, R. E., and W. R. Buck (1992), Crustal control of ridge segmentation inferred from observations of the Reykjanes Ridge, *Nature*, *357*, 583–586.

Bjarnason, I. T., W. Menke, O. Flóvenz, and D. Caress (1993), Tomographic imaging of the Mid-Atlantic plate boundary in southwestern Iceland, *J. Geophys. Res.*, *98*, 6607–6622.

Blichert-Toft, J., A. Agranier, M. Andres, R. Kingsley, J. Schilling, and F. Albarède (2005), Geochemical segmentation of the Mid-Atlantic Ridge north of Iceland and ridge–hot spot interaction in the North Atlantic, *Geochem. Geophys. Geosyst.*, *6*, Q01E19, doi:10.1029/2004GC000788.

Brandsdóttir, B., W. Menke, P. Einarsson, R. S. White, and R. K. Staples (1997), Färoe-Iceland Ridge Experiment: 2. Crustal structure of the Krafla central volcano, *J. Geophys. Res.*, *102*, 7867–7886.

Brandsdóttir, B., R. Detrick, N. Driscoll, and G. Kent (2001), Pilot study of the Tjörnes Fracture Zone, offshore Northern Iceland, using high-resolution multichannel seismic reflection profiling and CHIRP Sonar, *Eos Trans. AGU*, *82*(47), Abstract T42C-0949.

Brandsdóttir, B., et al. (2004), Tectonic details of the Tjörnes Fracture Zone, an onshore-offshore ridge-transform in N-Iceland, *Eos Trans. AGU*, *85*(47), Fall Meet. Suppl., Abstract T41A-1172.

Bunch, A. W. H., and B. L. N. Kennett (1980), The crustal structure of the Reykjanes Ridge at 59 30′N, *Geophys. J. R. Astron. Soc.*, *61*, 141–166.

Carlson, R. L., and G. S. Raskin (1984), Density of the ocean crust, *Nature*, *311*, 555–558.

Christeson, G. L., G. M. Purdy, and G. J. Fryer (1994), Seismic constraints on shallow crustal emplacement processes at the fast spreading East Pacific Rise, *J. Geophys. Res.*, *99*, 17,957–17,974.

Cochran, J. R., and M. Talwani (1978), Gravity anomalies, regional elevation, and the deep structure of the North Atlantic, *J. Geophys. Res.*, *83*, 4907–4924.

Creager, K. C., and L. M. Dorman (1982), Location of instruments on the seafloor by joint adjustment of instrument and ship positions, *J. Geophys. Res.*, *87*, 8379–8388.

Darbyshire, F., I. T. Bjarnason, R. S. White, and O. Flóvenz (1998), Crustal structure above the Iceland mantle plume imaged by the ICEMELT refraction profile, *Geophys. J. Int.*, *13*, 1131–1149.

Darbyshire, F. A., R. S. White, and K. F. Priestley (2000), Structure of the crust and uppermost mantle of Iceland from a combined seismic and gravity study, *Earth Planet. Sci. Lett.*, *181*(3), 409–428.

DeMets, C., R. G. Gordon, D. F. Argus, and S. Stein (1994), Effect of recent revision to the geomagnetic reversal time scale on estimates of current plate motions, *Geophys. Res. Lett.*, *21*, 2192–2194.

Detrick, R., J. Colling, R. Stephen, and S. Swift (1994), *In situ* evidence for the nature of the seismic layer 2/3 boundary in oceanic crust, *Nature*, *370*, 288–290.

Dilek, Y. (1998), Structure and tectonics of intermediate-spread oceanic crust drilled and DSDP/ODP holes 504B and 896A, Costa Rica Rift, in *Geological Evolution of Ocean Basins: Results From the Ocean Drilling Program*, edited by A. Cramp et al., *Geol. Soc. Spec. Publ.*, *131*, 179–197.

Foulger, G. R., et al. (2000), The seismic anomaly beneath Iceland extends down to the mantle transition zone and no deeper, *Geophys. J. Int.*, *143*(3), F2–F5.

Georgen, J. E., and J. Lin (2003), Plume-transform interactions at ultra-slow spreading ridges: Implications for the Southwest Indian Ridge, *Geochem. Geophys. Geosyst.*, *4*(9), 9106, doi:10.1029/2003GC000542.

Graham, D. W. (2002), Noble gas isotope geochemistry of mid-ocean ridge and ocean island basalts: Characterization of mantle source reservoirs, in *Noble Gases in Geochemistry and Cosmochemistry*, *Rev. Mineral. Geochem.*, vol. 47, edited by D. Porcelli, R. Wieler, and C. Ballentine, pp. 247–318, Mineral. Soc. Am., Washington, D. C.

Gudmundsson, O. (2003), The dense root of the Iceland crust, *Earth Planet. Sci. Lett.*, *206*, 427–440.

Gudmundsson, O., B. Brandsdóttir, W. Menke, and G. E. Sigvaldson (1994), The crustal magma chamber of the Katla volcano in South Iceland revealed by 2-D seismic undershooting, *Geophys. J. Int.*, *119*, 277–296.

Gunnarsson, K. (1998), Sedimentary basins of the north Iceland Shelf, 43 pp., draft report, *OS-98014*, Orkustofnun (Natl. Energy Auth.), Reykjavík.

Haigh, B. I. R. (1973), North Atlantic oceanic topography and lateral variations in the upper mantle, *Geophys. J. R. Astron. Soc.*, *33*, 405–420.

Hanan, B., and J.-G. Schilling (1997), The dynamic evolution of the Iceland mantle plume: The lead isotope perspective, *Earth Planet. Sci. Lett.*, *151*, 43–60.

Harding, A. J., G. M. Kent, and J. A. Orcutt (1993), A multichannel seismic investigation of the upper crustal structure at 9°N on the East Pacific Rise: Implications for crustal accretion, *J. Geophys. Res.*, *98*, 13,925–13,944.

Hart, S. R., J.-G. Schilling, and J. L. Powell (1973), Basalts from Iceland and along the Reykjanes Ridge: Sr isotope geochemistry, *Nature*, *246*, 565–571.

Holbrook, W. S., et al. (2001), Mantle thermal structure and melting processes during continental breakup in the North Atlantic, *Earth Planet. Sci. Lett.*, *190*, 251–266.

Hooft, E. E. E., R. S. Detrick, D. R. Toomey, J. A. Collins, and J. Lin (2000), Crustal thickness and structure along the axial valley of three contrasting spreading segments of the Mid-Atlantic Ridge, 33.5°–35°N, *J. Geophys. Res.*, *105*, 8205–8226.

Houtz, R. E. (1976), Seismic properties of layer 2A in the Pacific, *J. Geophys. Res.*, *81*, 6321–6340.

Houtz, R., and J. Ewing (1976), Upper crustal structure as a function of plate age, *J. Geophys. Res.*, *81*, 2490–2498.

Hung, S., Y. Shen, and L. Chiao (2004), Imaging seismic velocity structure beneath the Iceland hot spot: A finite frequency approach, *J. Geophys. Res.*, *109*, B08305, doi:10.1029/2003JB002889.

Ito, G., and J. J. Mahoney (2005), Flow and melting of a heterogeneous mantle: 1. Method and importance to the geochemistry of ocean island and mid-ocean ridge basalts, *Earth Planet. Sci. Lett.*, *230*, 29–46.

Ito, G., J. Lin, and C. W. Gable (1996), Dynamics of mantle flow and melting at a ridge-centered hotspot: Iceland and the Mid-Atlantic Ridge, *Earth Planet. Sci. Lett.*, *144*, 53–74.

Ito, G., Y. Shen, G. Hirth, and C. J. Wolfe (1999), Mantle flow, melting, and dehydration of the Iceland plume, *Earth Planet. Sci. Lett.*, *165*, 81–96.

Jull, M., and P. B. Kelemen (2001), On the condition for lower crustal convective instability, *J. Geophys. Res.*, *106*, 6423–6446.

Jung, W.-Y., and P. R. Vogt (1997), A gravity and magnetic anomaly study of the extinct Aegir Ridge, Norwegian Sea, *J. Geophys. Res.*, *102*, 5065–5089.

Kaban, M. K., O. G. Flovenz, and G. Palmason (2002), Nature of the crust-mantle transition zone and the thermal state of the upper mantle beneath Iceland from gravity modeling, *Geophys. J. Int.*, *149*, 281–299.

Klein, E. M., and C. H. Langmuir (1987), Global correlations of ocean ridge basalt chemistry with axial depth and crustal thickness, *J. Geophys. Res.*, *92*, 8089–8115.

Kodaira, S., R. Mjelde, K. Gunnarsson, H. Shiobara, and H. Shimamura (1997), Crustal structure of the Kolbeinsey Ridge, North Atlantic, obtained by use of ocean bottom seismographs, *J. Geophys. Res.*, *102*, 3131–3151.

Korenaga, J., W. S. Holbrook, G. M. Kent, P. B. Kelemen, R. S. Detrick, H.-C. Larsen, J. R. Hopper, and T. Dahl-Jensen (2000), Crustal structure of the southeast Greenland margin from joint refraction and reflection seismic tomography, *J. Geophys. Res.*, *105*, 21,591–21,614.

Korenaga, J., W. S. Holbrook, R. S. Detrick, and P. B. Kelemen (2001), Gravity anomalies and crustal structure of the southeast Greenland margin, *J. Geophys. Res.*, *106*, 8853–8870.

Langmuir, C. H., E. M. Klein, and T. Plank (1992), Petrological constraints on melt formation and migration beneath midocean ridges, in *Mantle Flow and Melt Generation at Mid-Ocean Ridges*, *Geophys. Monogr. Ser.*, vol. 71, edited by J. Phipps Morgan, D. Blackman, and J. L. Sinton, pp. 183–280, AGU, Washington, D. C.

McKenzie, D., and M. J. Bickle (1988), The volume and composition of melt generated by extension of the lithosphere, *J. Petrol.*, *29*, 625–679.

Menke, B. (1999), Crustal isostasy indicates anomalous densities beneath Iceland, *Geophys. Res. Lett.*, *26*, 1215–1218.

Menke, W., and V. Levin (1994), Cold crust in a hot spot, *Geophys. Res. Lett.*, *21*, 1967–1970.

Menke, W., B. Brandsdóttir, P. Einarsson, and I. Bjarnasson (1996), Reinterpretation of the RRISP-77 Iceland shear wave profiles, *Geophys. J. Int.*, *126*, 166–172.

Menke, W., M. West, B. Brandsdóttir, and D. Sparks (1998), Compressional and shear velocity structure of the lithosphere in northern Iceland, *Bull. Seismol. Soc. Am.*, *88*, 1561–1571.

Mertz, D. F., C. W. Devey, W. Todt, P. Stoffers, and A. W. Hoffman (1991), Sr-Nd-Pb isotope evidence against plume-

asthenosphere mixing north of Iceland, *Earth Planet. Sci. Lett.*, *25*, 411–414.
Moser, T. J. (1991), Shortest path calculation of seismic rays, *Geophysics*, *56*, 59–67.
Moser, T. J., G. Nolet, and R. Snieder (1992), Ray bending revisited, *Bull. Seismol. Soc. Am.*, *82*, 259–288.
Navin, D. A., C. Peirce, and M. C. Sinha (1998), The RAMESSES experiment - II. Evidence for accumulated melt beneath a slow spreading ridge from wide-angle refraction and multichannel reflection seismic profiles, *Geophys. J. Int.*, *135*, 746–772.
Olafsson, S., R. Sigbjornsson, and P. Einarsson (1998), Estimation of source parameters and Q from acceleration recorded in the Vatnafjoll earthquake in South Iceland, *Bull. Seismol. Soc. Am.*, *88*, 556–563.
Paige, C. C., and M. A. Saunders (1982), LSQR: An algorithm for sparse linear equations and least squares, *ACM Trans. Math. Software*, *8*, 43–71.
Parker, R. L., and S. P. Huestis (1974), The inversion of magnetic anomalies in the presence of topography, *J. Geophys. Res.*, *79*, 1587–1594.
Poreda, R. J., J.-G. Schilling, and H. Craig (1986), Helium and hydrogen isotopes in ocean-ridge basalts north and south of Iceland, *Earth Planet. Sci. Lett.*, *113*, 129–144.
Sæmundsson, K. (1978), Fissure swarms and central volcanoes of the neovolcanic zones of Iceland, *Geol. J.*, *10*, spec. issue, 415–432.
Schilling, J.-G. (1973a), Iceland mantle plume, *Nature*, *246*, 141–143.
Schilling, J.-G. (1973b), Iceland mantle plume: Geochemical study of Reykjanes Ridge, *Nature*, *242*, 565–571.
Schilling, J.-G. (1999), Dispersion of the Jan Mayen and Iceland mantle plumes in the Arctic: A He-Pb-Nd-Sr isotope tracer study of basalts from the Kolbeinsey, Mohns, and Knipovich Ridges, *J. Geophys. Res.*, *104*, 10,543–10,569.
Schilling, J.-G., M. Zajac, R. Evans, T. Johnston, W. White, J. Devine, and R. Kingsley (1983), Petrologic and geochemical variations along the Mid-Atlantic Ridge from 29°N to 73°N, *Am. J. Sci.*, *283*, 510–586.
Shen, Y., and D. W. Forsyth (1995), Geochemical constraints on initial and final melting beneath mid-ocean ridges, *J. Geophys. Res.*, *100*, 2211–2237.
Shen, Y., S. C. Solomon, I. T. Bjarnason, and C. J. Wolfe (1998), Seismic evidence for a lower mantle origin of the Iceland mantle plume, *Nature*, *395*, 62–65.
Shen, Y., et al. (2002), Seismic evidence for a tilted mantle plume and north-south mantle flow beneath Iceland, *Earth Planet. Sci. Lett.*, *197*, 261–272.
Smallwood, J., and R. S. White (1998), Crustal accretion at the Reykjanes Ridge, 61–62°N, *J. Geophys. Res.*, *103*, 5185–5201.
Smith, W. H. F., and D. T. Sandwell (1997), Global seafloor topography from satellite altimetry and ship depth soundings, *Science*, *277*, 1957–1962.
Staples, R. K., R. S. White, B. Brandsdóttir, W. Menke, P. K. H. Maguire, and J. H. McBride (1997), Färoe-Iceland Ridge Experiment: 1. Crustal structure of northeastern Iceland, *J. Geophys. Res.*, *101*, 7849–7866.
Talwani, M., and O. Eldholm (1977), Evolution of the Norwegian-Greenland Sea, *Geol. Soc. Am. Bull.*, *8*, 969–999.
Talwani, M., C. C. Windisch, and M. G. Langseth (1971), Reykjanes ridge crest: A detailed geophysical study, *J. Geophys. Res.*, *76*, 473–517.
Toomey, D. R., G. M. Purdy, S. C. Solomon, and W. S. D. Wilcock (1990), The three-dimensional seismic velocity structure of the East Pacific Rise near latitude 9°30′N, *Nature*, *347*, 639–645.
Vera, E. E., J. C. Mutter, P. Buhl, J. A. Orcutt, A. J. Harding, M. E. Kappus, R. S. Detrick, and T. M. Brocher (1990), The structure of 0- to 0.2-m.y.-old oceanic crust at 9°N on the East Pacific Rise from expanded spread profiles, *J. Geophys. Res.*, *95*(B10), 15,529–15,556.
Vogt, P. R. (1983), The Iceland mantle plume: Status of the hypothesis after a decade of new work, in *Structure and Development of the Greenland-Scotland Ridge*, edited by M. H. P. Bott et al., pp. 191–213, Springer, New York.
Vogt, P. R., G. L. Johnson, and L. Kristjanssn (1980), Morphology and magnetic anomalies north of Iceland, *J. Geophys.*, *47*, 67–80.
Weir, N., R. S. White, B. Brandsdóttir, P. Einarsson, H. Shimamura, and H. Shiobara (2001), Crustal structure of the northern Reykjanes Ridge and Reykjanes Peninsula, south-west Iceland, *J. Geophys. Res.*, *106*, 6347–6368.
White, R. S. (1993), Melt production rates in mantle plumes, *Philos. Trans. R. Soc. London, Ser. A*, *342*, 137–153.
White, R. S., J. W. Brown, and J. R. Smallwood (1995), The temperature of the Iceland plume and origin of outward propagating V-shaped ridges, *J. Geol. Soc. London*, *152*, 1039–1045.
Wolfe, C. J., I. T. Bjarnason, J. C. VanDecar, and S. C. Solomon (1997), Seismic structure of the Iceland mantle plume, *Nature*, *385*, 245–247.
Yale, M. M., and J. Phipps Morgan (1998), Asthenosphere flow model of hotspot-ridge interactions: A comparison of Iceland and Kerguelen, *Earth Planet. Sci. Lett.*, *161*, 45–56.